On the spatiotemporal variability of soil moisture and evapotranspiration in a mountainous basin within the North American monsoon region

Enrique R. Vivoni,[1] Julio C. Rodríguez,[2] and Christopher J. Watts[3]

Received 25 May 2009; revised 11 August 2009; accepted 5 October 2009; published 10 February 2010.

[1] In the North American monsoon (NAM) region, in-phase seasonality in precipitation and radiation should lead to corresponding changes in the catchment hydrologic response and its spatiotemporal variability. Nevertheless, relatively little is known on the catchment response in the NAM region because of the paucity of observations. Numerical watershed models, tested against field and remote sensing data, can aid in identifying catchment hydrologic patterns and the controls exerted by climate, soil, vegetation, and terrain properties. In this study, we utilize a distributed hydrologic model to explore the soil moisture and evapotranspiration distributions in a semiarid mountain basin. Results indicate a reliable and consistent model performance at the point and catchment scales for a set of tested hydrologic states and fluxes. Distributed model simulations reveal that soil, vegetation, and terrain controls on catchment spatial patterns vary according to the wetness state in a manner similar to that found across a wider range of climate conditions. Spatiotemporal variations in soil moisture and evapotranspiration exhibit hysteresis as an emergent pattern induced by climate variability and the underlying hydrologic interactions in the catchment.

Citation: Vivoni, E. R., J. C. Rodríguez, and C. J. Watts (2010), On the spatiotemporal variability of soil moisture and evapotranspiration in a mountainous basin within the North American monsoon region, *Water Resour. Res.*, *46*, W02509, doi:10.1029/2009WR008240.

1. Introduction

[2] The North American monsoon (NAM) is an atmospheric circulation pattern that leads to an in-phase relation between solar radiation and precipitation in the southwestern United States and northwest Mexico from July to September [*Adams and Comrie*, 1997; *Sheppard et al.*, 2002]. Local and mesoscale convective storms during the NAM account for a large percentage of the annual precipitation, ranging from 40% to 80% in the region [*Douglas et al.*, 1993]. The seasonal coupling of precipitation and solar radiation is responsible for significant changes in landscape characteristics during the NAM, including the greening of drought-deciduous ecosystems [e.g., *Salinas-Zavala et al.*, 2002; *Watts et al.*, 2007; *Vivoni et al.*, 2008b; *Méndez-Barroso et al.*, 2009]. Strong variations in land surface and ecosystem conditions occur within several days after the NAM onset. Ecosystem seasonality also induces changes in albedo, soil temperature, and evapotranspiration, which impact the energy balance [e.g., *Small and Kurc*, 2003; *Watts et al.*, 2007; *Vivoni et al.*, 2008b; *Méndez-Barroso and Vivoni*, 2010]. Relatively less is known on the seasonality of the water balance, though *Gochis et al.* [2006] identified that up to 85% of the annual streamflow occurs in response to the NAM.

[3] Seasonal precipitation during the NAM is mediated by soil, topographic, and vegetation conditions that partition rainfall into evapotranspiration, streamflow, and changes in catchment storage. Seasonal precipitation leads to (1) increases in streamflow in ephemeral rivers [*Brito-Castillo et al.*, 2003; *Gochis et al.*, 2006] and (2) increases in plant biomass that promote evapotranspiration [*Vivoni et al.*, 2008b; *Dominguez et al.*, 2008]. Catchment storages, including root zone soil moisture and groundwater levels, should also increase in response to the NAM. For example, monthly runoff ratio estimates in basins of northwest Mexico increase from July to October, likely because of higher antecedent wetness [*Gochis et al.*, 2006]. However, given the paucity and low quality of long-term observations in northwest Mexico [*Mora and Iverson*, 1998; *Higgins et al.*, 2003], quantifying the catchment water balance in this important area of the NAM region is not a simple task. In this respect, numerical models, tested against limited data sets, can help constrain estimates of the spatiotemporal variability in catchment hydrology and identify the controls exerted by climate, soil, vegetation, and topographic properties.

[4] The spatiotemporal variability of catchment hydrologic processes in northwest Mexico is due to several factors: (1) the seasonal evolution of ecosystem properties, including changes in surface albedo [*Salinas-Zavala et al.*, 2002; *Méndez-Barroso and Vivoni*, 2010], and biomass/leaf area index [*Maass et al.*, 1995; *Watts et al.*, 2007], among

[1]School of Earth and Space Exploration and School of Sustainable Engineering and the Built Environment, Arizona State University, Tempe, Arizona, USA.
[2]Departamento de Agricultura y Ganadería, Universidad de Sonora, Hermosillo, Mexico.
[3]Departamento de Física, Universidad de Sonora, Hermosillo, Mexico.

0043-1397/10/2009WR008240$09.00

others, and (2) the complex topography and its role in the spatial distribution of precipitation [*Negri et al.*, 1993; *Gochis et al.*, 2004], plant functional types and communities [*Coblentz and Riitters*, 2004; *Vivoni et al.*, 2007b], and soil properties [*Wierenga et al.*, 1987; *Descroix et al.*, 2002a]. As a result, quantifying the variability of hydrologic conditions through observations alone is difficult in the mountainous terrain of the NAM region. Nevertheless, *Vivoni et al.* [2008a] used ground and remotely sensed estimates of surface soil moisture to reveal topographic controls, suggesting that capturing terrain features is important in numerical models of northwest Mexico.

[5] Among the catchment water balance components, soil moisture is a key as it mediates the partitioning of infiltration and runoff [e.g., *Goodrich et al.*, 1994; *Descroix et al.*, 2002b] and it limits evapotranspiration from soil and vegetation [e.g., *Kurc and Small*, 2004; *Vivoni et al.*, 2008b]. As a result, quantifying the spatiotemporal patterns of soil moisture is an effective means to summarize catchment hydrologic conditions [*Western et al.*, 1999; *Ivanov et al.*, 2004b; *Settin et al.*, 2007]. Unfortunately, at present, observed or model-derived soil moisture data sets in the NAM region are limited to coarse spatial resolutions inadequate for catchment studies [*Mesinger et al.*, 2006; *Zhu and Lettenmaier*, 2007]. For instance, the North American Regional Reanalysis (NARR) soil moisture products at 32 km resolution have significant biases [*Mo*, 2008; *Vivoni et al.*, 2008b]. High-resolution soil moisture observations during field campaigns, such as the Soil Moisture Experiment–North American Monsoon in 2004 (SMEX04-NAME) [*Higgins and Gochis*, 2007; *Bindlish et al.*, 2008], can help address this limitation by providing estimates that can be used to test detailed numerical watershed models.

[6] It is important to identify the controls on soil moisture spatiotemporal patterns as these provide a basis for improved predictions. For example, *Lawrence and Hornberger* [2007] suggested that climate dictates whether vegetation (semiarid), terrain (temperate), or soil (humid) properties determine soil moisture variability. Other studies have also investigated controls on soil moisture distributions using field or remote sensing data [e.g., *Rodríguez-Iturbe et al.*, 1995, *Grayson et al.*, 1997; *Crave and Gascuel-Odoux*, 1997; *Kim and Barros*, 2002; *Wilson et al.*, 2004]. *Mahmood and Vivoni* [2008] used a watershed model, tested against the spatial observations of *Vivoni et al.* [2008c], to reveal the contributions from catchment fluxes (e.g., evapotranspiration, rainfall, and lateral fluxes) on the soil moisture patterns in a forested, mountain basin. Model-based studies of soil moisture variability also provide a means to explore the mechanisms underlying the spatial patterns [e.g., *Peters-Lidard et al.*, 2001; *Grayson et al.*, 2002; *Crow et al.*, 2005]. In northwest Mexico, landscape seasonality and complex terrain provide a challenging environment for quantifying the evolution of soil moisture patterns and identifying its controls.

[7] In this study, we utilize a distributed hydrologic model to explore the spatiotemporal variability and controls on soil moisture and evapotranspiration distributions in a complex basin in northwest Mexico (92.5 km^2). Our approach is based on using field and remote sensing observations from SMEX04-NAME to both parameterize and test a numerical model. We utilize the triangulated irregular network (TIN)-based Real-time Integrated Basin Simulator (tRIBS) [*Ivanov et al.*, 2004a; *Vivoni et al.*, 2007a] to conduct two types of simulations: (1) 1-D (vertical) modeling at an eddy covariance (EC) tower site ($\sim$100 m^2), and (2) 3-D simulations in a mid-size mountain basin spanning an elevation transect (92.5 km^2). These simulations are conducted during a single NAM season in 2004 to take advantage of the available SMEX04-NAME data sets. Both simulation domains are within the Río San Miguel basin in northern Sonora, Mexico, and have been the focus of intensive field observations [e.g., *Watts et al.*, 2007; *Vivoni et al.*, 2007b, 2008a, 2010] and remote sensing data analyses [*Vivoni et al.*, 2008a, *Méndez-Barroso et al.*, 2009; *Méndez-Barroso and Vivoni*, 2010]. Detailed modeling efforts such as this are essential for developing predictive skill in hydrologic forecasts of mountainous basins exhibiting high landscape seasonality in the NAM region.

[8] This paper is organized as follows. Section 2 describes the study region and modeling domains, with emphasis placed on the SMEX04-NAME data sets. This section also describes the distributed hydrologic model parameterization. In section 3, we compare model simulations with soil moisture observations at the EC site and in the mountain basin. We then utilize the tested numerical model to explore controls on the soil moisture and evapotranspiration spatiotemporal variability and organization. We discuss and synthesize our modeling results in section 4 in light of the emergent behavior arising from complex catchment patterns to guide efforts that improve regional-scale predictions. Finally, section 5 summarizes the study conclusions.

2. Methods

2.1. Study Region and Its Characteristics

[9] The study region is located in northern Sonora, Mexico, in a rural area characterized by ephemeral rivers and complex terrain [*Vivoni et al.*, 2007b]. Figure 1 depicts the study location, along with the two modeling domains: (1) an EC tower at Rayón, Sonora, and (2) the Sierra Los Locos (SLL) basin near Opodepe, Sonora. Site climate is considered steppe or semi-arid (BSh), according to the Köppen-Geiger classification [*Peel et al.*, 2007], characterized by hot, arid conditions, and winter temperatures above 0°C. A defining feature is the seasonal precipitation regime with 60–70% of the annual total during the NAM and a weaker, winter precipitation season [*Vivoni et al.*, 2008b]. Mean annual precipitation (±1 SD) at the Cucurpe, Meresichic, and Rayón sites was 564 ± 158, 496 ± 204, and 481 ± 181 mm/yr, over 1981–2006. Thus, the mean annual precipitation varies from $\sim$400 to 600 mm/yr, depending on the latitude and elevation, though long-term data sets at high elevations are not available.

[10] Figure 1b presents the regional terrain and hydrographic features of the Río San Miguel basin (3796 km^2). The north–south basin orientation above the El Cajón gauging site is due to the long, parallel mountain ranges [e.g., *Coblentz and Riitters*, 2004]. Elevation varies from $\sim$400 to 2000 m, slopes range from 0 to 56° (mean slope of 5.5°) and aspects are primarily east- and west-facing (from analysis of 29 m resolution terrain data from *Instituto Nacional de Estadística, Geografía e Informática* (*INEGI*)

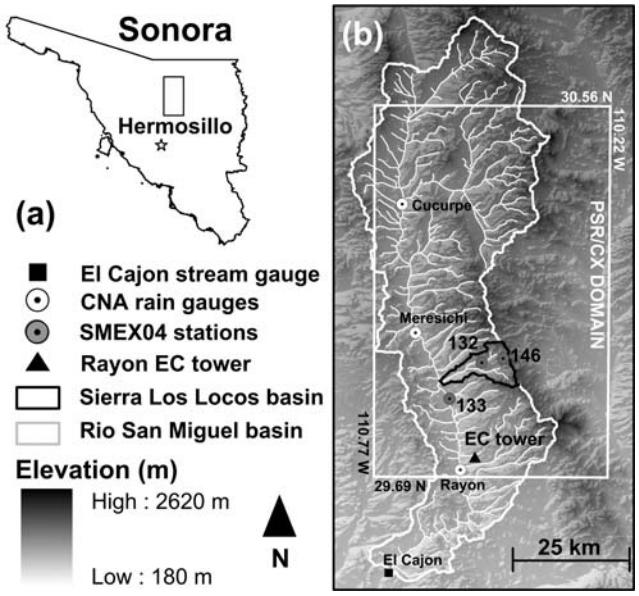

Figure 1. (a) Study region location in northern Sonora and (b) its characteristics including, digital elevation model (DEM), basin boundaries for Río San Miguel and Sierra Los Locos (SLL), stream networks, and measurement locations (continuous stations 132, 133, and 146).

[1998]). Basin landforms include: (1) alluvial valleys, (2) dissected foothills and piedmonts, and (3) rugged slopes with exposed rock. Basin geology is complex with mountains consisting of Mesozoic granites, Cenozoic conglomerates, and Tertiary rhyolites, while Quaternary alluvium and Mesozoic limestones are found in valley bottoms [*Secretaría de Programación y Presupuesto*, 1984]. Soil distributions and their properties are strongly related to landform characteristics and the underlying parent material. Soil types include: lithosols (I), eutric regosols (Re), eutric fluvisols (Je), haplic yermosols (Yh), haplic phaeozems (Hh), and luvic xerosols (Xl) [*Instituto Nacional de Investigaciones Forestales, Agrícolas y Pecuarias* (*INIFAP*), 2001].

[11] Ecosystem distributions are linked to elevation because of temperature and precipitation gradients along mountain fronts. *Vivoni et al.* [2007b] and *Méndez-Barroso and Vivoni* [2010] describe the plant communities in the region. The major ecosystems include (in order from low to high elevation): (1) Irrigated agriculture primarily peanuts, alfalfa, and vegetables, (2) Sonoran riparian deciduous woodland, (3) Sonoran desert scrub, (4) Sinaloan thorn scrub, (5) Sonoran savanna grassland, (6) Madrean evergreen woodland, and (7) Madrean montane conifer. Low elevations ($\sim$400–600 m) consist of Sonoran desert scrub with low-branching trees and shrubs, interspersed with bare ground. The Sinaloan thorn scrub (subtropical scrubland) occurs at intermediate elevations ($\sim$600–900 m) and is composed of thorny, drought-deciduous trees and shrubs. Mountain tops are primarily Madrean evergreen woodlands or conifer forests (oak savannas or evergreen forests) consisting of stands of a variety of oak or conifer species interspersed with grasslands ($\sim$900–1600 m). These four ecosystems occupy the SLL basin, while the EC site is a Sinaloan thorn scrub ecosystem.

2.2. Field and Remote Sensing Observations During SMEX04-NAME

[12] SMEX04-NAME was designed to provide ground- and aircraft-based observations during the 2004 monsoon. Sampling efforts were carried out in the Río San Miguel, including: (1) deployment of a continuous network of precipitation and soil moisture stations (14 sites), (2) manual sampling of soil moisture along a topographic transect in the SLL basin (30 sites), (3) establishment of an EC tower, (4) aircraft-based soil moisture retrievals using the Polarimetric Scanning Radiometer (PSR/CX), and (5) ancillary data collection such as soil and vegetation sampling (see Figure 1 for location of EC site, PSR/CX domain and three stations).

[13] Individual components of the SMEX04-NAME experiment varied in duration with the best overlap from late July to mid-August. We focus on the period from 23 July to 30 September 2004 on the basis of available forcing and validation data at the EC site. Figure 2 depicts EC-site observations, including precipitation from a tipping-bucket rain gauge (Hydrological Services TB3), soil moisture (θ, %) at 5 cm depth (Stevens Hydra sensor), and the evaporative fraction (EF) defined as the ratio of the latent heat flux (λE) to the total turbulent fluxes [$EF = \lambda E/(\lambda E + H)$], where H is the sensible heat flux. The eddy-covariance technique is used to estimate EF from data collected from a 3-D sonic anemometer (Campbell CSAT3) and a hygrometer (LI-COR L17500) located above the tree canopies at 8 m height (see section 2.4 for a description of the site ecosystem). We used EC methods discussed by *Scott et al.* [2004] and *Watts et al.* [2007] to process the high-frequency measurements and obtain 30 min surface flux estimates in the $\sim$100 m^2 footprint region around the site [also see *Vivoni et al.*, 2010].

[14] Figure 2 illustrates the strong relation between precipitation, surface soil moisture, and EF. The study extent allows examining four wet periods in terms of soil moisture, each lasting several days, separated by intervening soil moisture dry-downs. Each wet period is accompanied by an increase in EF, indicating a greater evapotranspiration relative to the total turbulent fluxes ($\lambda E + H$), while dry-downs are accompanied by an increase in H and reductions in EF. During these wetting and drying episodes, the Normalized Difference Vegetation Index (NDVI) from the Moderate Resolution Imaging Spectroradiometer (MODIS), in the 250 m pixel co-located at the EC site (from *Méndez-Barroso et al.* [2009]), shows the plant canopy was at maximum development, with decreasing greenness toward the end of September. As a result, the effects of the rapid greening process in early July (NDVI increase from 0.19 to 0.54) are minimized during this period at the EC site. Thus, within the range of NDVI changes at the site [*Méndez-Barroso et al.*, 2009], the observed variations near full canopy development are minor. This justifies the treatment of vegetation as temporally constant in the point and catchment-scale simulations presented here, though spatial variability in vegetation is captured in the SLL basin.

[15] The SLL basin has a high spatial variability in land surface properties (Figure 3). A 29 m resolution digital elevation model (DEM) was processed to obtain the boundary and stream network for the basin [*INEGI*, 1998]. Elevations in the basin range from 657 to 1681 m, with a

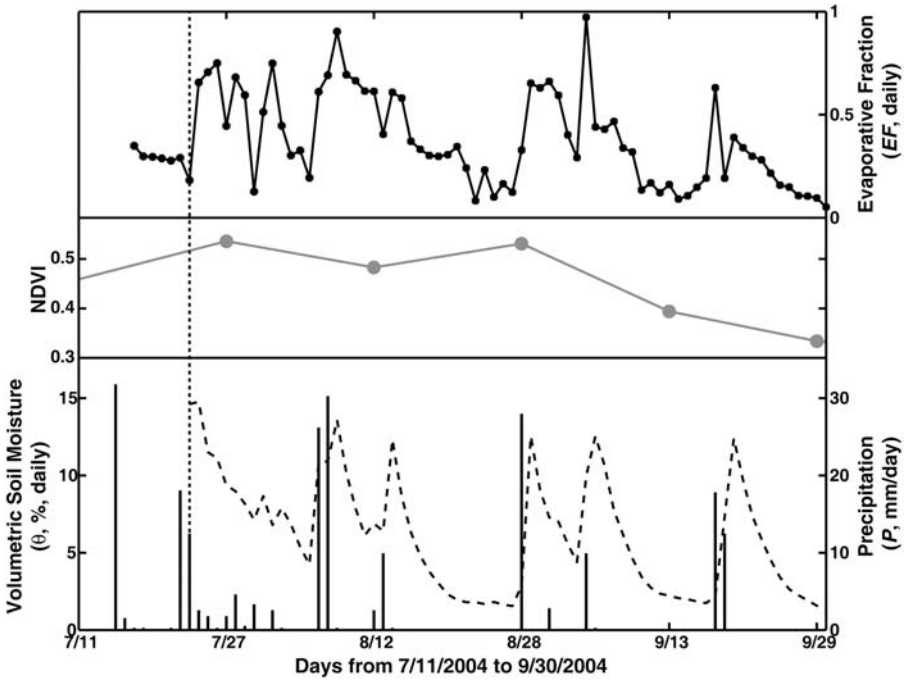

Figure 2. EC site observations during 2004 monsoon including: daily evaporative fraction (EF), NDVI (MODIS 16 day composites in 250 m pixel at EC site), daily averaged volumetric soil moisture at 5 cm depth (θ in %, dashed line), and daily precipitation (P in mm/d, black bars). Vertical dashed line depicts the start of simulation period. For reference, the NDVI is 0.19 and 0.3 prior to and after the NAM (not shown).

mean height of 1045.4 ± 226.2 m and a mean slope of 16.4° ± 10.0°. Surface soil texture is available as coarse polygon data from the U.N. Food and Agriculture Organization (FAO) [*INIFAP*, 2001]. On the basis of field soil texture at 55 sites, we developed and tested a simple approach to condition the FAO classes on slope intervals (0–5°, 5–10°, 10–20°, 20–30°, >30°). The method captured hillslope soil processes with finer textures (e.g., sandy clay loam) in flat areas and coarser soils (e.g., sand or exposed rock) in high-slope regions. Similarly, vegetation maps are available as coarse land use land cover (LULC) polygons [*Secretaría de Infraestructura Urbana y Ecología–Instituto del Medio Ambiente y Desarrollo Sustentable del Estado de Sonora*, 1998]. Nevertheless, *Yilmaz et al.* [2008] developed and tested a vegetation classification for the study region using 30 m Landsat 5 Thematic Mapper scenes, which is used here for the numerical simulations. The method captured the location of grassland, subtropical scrubland, oak savanna, and evergreen forests within the LULC polygons. While the elevation, surface soil texture and vegetation fields are the best available products in the region, these may contain artifacts (e.g., interpolation errors in the DEM because of contouring) which may impact the numerical simulations.

[16] SMEX04-NAME data near the SLL basin consisted of the following. Three stations were installed (132, 133, and 146) with a tipping-bucket rain gauge (Texas Electronics TR525I) and two Hydra sensors. The soil dielectric sensor measured volumetric soil moisture and temperature at 5 cm depth using a sand calibration [*Seyfried and Murdock*, 2004]. Thirty sampling plots were established along an elevation transect for soil moisture sampling. A Theta probe (Delta-T devices) was used to estimate volumetric soil moisture from a factory calibration for mineral soil, with an accuracy of ±0.05 m^3/m^3 [*Cosh et al.*, 2005], and found to be appropriate for the sampling locations [*Vivoni et al.*, 2007b]. Five, daily samples were taken in each ~2 × ~2 m^2 plot over a 0–6 cm depth. *Vivoni et al.* [2007b] found good agreement in the Hydra sensor, Theta probe and gravimetric samples at station 146. Figure 3d compares the transect soil moisture data to retrievals from the PSR/CX sensor, a four-channel microwave imager [*Jackson et al.*, 2005]. The aircraft sensor was flown during 11 days in August 2004. PSR/CX data was processed into a 7.32H GHz brightness temperature and converted to an 800 m volumetric soil moisture field [*Bindlish et al.*, 2008].

2.3. Distributed Hydrologic Model

[17] Numerical simulations were carried out in the two modeling domains using tRIBS, a fully distributed, physically based model of hydrologic processes [*Ivanov et al.*, 2004a; *Vivoni et al.*, 2007a]. The model has a spatially explicit treatment of basin heterogeneities in topography, soils, vegetation, and atmospheric forcing. A catchment is represented by a TIN consisting of elevation, channel, and boundary nodes, which capture basin features with a reduced number of elements [*Vivoni et al.*, 2004]. In tRIBS, Voronoi polygons are uniquely associated with each TIN node and serve as the finite-volume domain for calculations. The model accounts for a range of hydrologic processes that track the catchment response, including: (1) canopy interception; (2) evapotranspiration from bare soil and vegetated surfaces; (3) infiltration and soil moisture redistribution; (4) shallow subsurface transport; and (5) overland and channel flow. Alternative domain configurations are possible

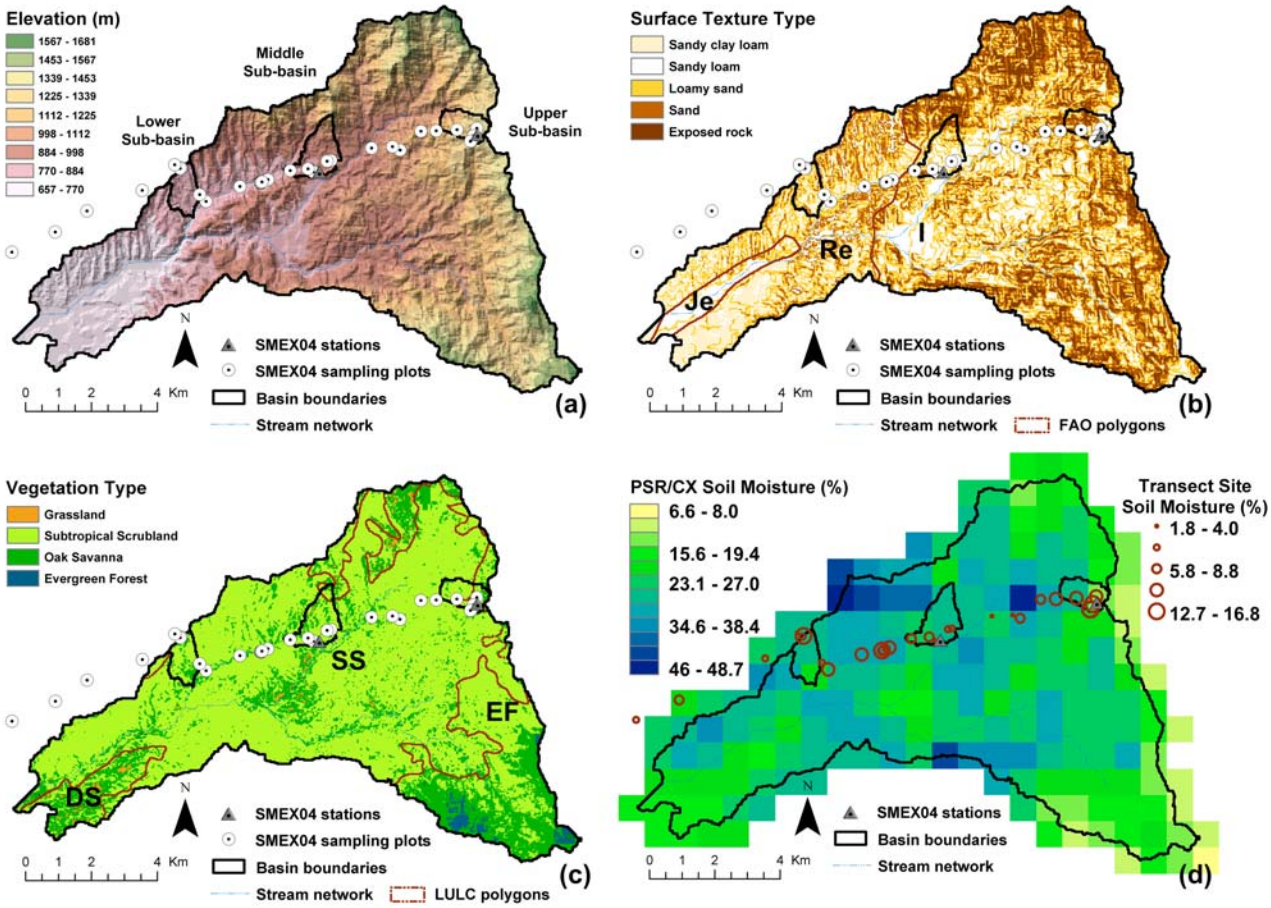

Figure 3. Sierra Los Locos characteristics, including (a) TIN derived from the 29 m DEM, (b) surface soil texture (29 m slope-texture approach with the FAO polygons: I, lithisols; Re, eutric regosols; Je, eutric fluvisols), (c) vegetation (30 m Landsat 5 TM approach with the LULC polygons: EF, evergreen forest; SS, subtropical scrubland; DS, desert scrubland), and (d) comparison of PSR/CX and sampling plot volumetric soil moisture (%) for 5 August 2004.

allowing simulations of individual soil columns, hillslopes, or complex, 3-D landscapes. Additional details on the model physics can be found in the studies of *Ivanov et al.* [2004a] and *Vivoni et al.* [2007a].

[18] Given the emphasis of this study, we briefly describe the soil moisture dynamics in the distributed model. Each Voronoi polygon consists of a sloped, heterogeneous soil column above an impermeable layer. A kinematic approximation for unsaturated flow is used to compute infiltration [*Cabral et al.*, 1992; *Garrote and Bras*, 1995; *Ivanov et al.*, 2004a]. Single infiltration fronts interact with the pre-storm moisture profile, determined from hydrostatic equilibrium, and the water table position. This interaction leads to a range of possible soil moisture states, which influence infiltration and runoff. Soil evaporation and plant transpiration are extracted according to atmospheric demand, derived from energy balance calculations using the Penman-Monteith combination equation, and soil moisture availability (see *Ivanov et al.* [2004a] for details on the evapotranspiration calculations). Coupled to the vertical dynamics is lateral redistribution in the vadose zone and shallow aquifer driven by surface topography or water table gradients.

2.4. Point and Catchment-Scale Model Applications

[19] TIN domains for the simulations at the EC site and SLL basin were derived using topographic data from *INEGI* [1998]. A single, hexagonal Voronoi polygon was specified for the EC site (29.74°N, 110.54°W, 632 m), with a total area of 98.77 m^2. A flat element was assumed on the basis of the position of the tower on the alluvial fan surface. A 1 m soil depth was used based on a soil pit excavated near the tower. Soil analyses indicate a sandy loam texture in the top 30 cm and a sandy clay loam in the lower profile (soil classified as eutric regosols, Re). The EC site is classified as a Sinaloan thorn scrub with a mixture of trees, shrubs, and cacti, interspersed by bare soil. The main species are mesquite (*Prosopis juliflora*), organ pipe cactus (*Stenocereus thurberi*), whiteball acacia (*Acacia angustissima*), tree ocotillo (*Fouquieria macdougalii*), and paloverde (*Cercidium sonorae*). As shown by *Méndez-Barroso and Vivoni* [2010], the EC site is representative of a larger subtropical scrubland region.

[20] The SLL domain was derived using the hydrographic TIN procedure of *Vivoni et al.* [2004], which preserves the nodes that minimize the difference between the TIN and the original DEM for an error tolerance, z_r. The TIN also includes the basin boundary, stream network and a

Table 1. Model Parameters for EC Site Simulations[a]

Parameter	Variable (Unit)	Value	Source
Saturated hydraulic conductivity	K_s (mm/hr)	25.0	1
Soil porosity	n (dimensionless)	0.45	1
Saturated soil moisture content	θ_s (dimensionless)	0.41	1
Residual soil moisture content	θ_r (dimensionless)	0.02	2
Stress soil moisture content	θ^* (dimensionless)	0.18	3
Pore size distribution index	m (dimensionless)	0.85	4
Soil heat conductivity	k_s (J/msK)	0.2	5
Soil heat capacity	C_s (J/m^{3}K)	1.61×10^6	6
Soil depth	Z_r (m)	1.0	7
Surface emissivity	E_s (dimensionless)	0.98	8
Vegetation fraction	v (dimensionless)	0.60	9
Albedo	a (dimensionless)	0.16	8
Vegetation height	h (m)	6.0	9
Vegetation transmission	K_t (dimensionless)	0.95	10
Minimum stomatal resistance	r_{min} (s/m)	20	11

[a]Sources for model parameters are as follows: 1, *Rawls et al.* [1983] with modifications on the basis of soil analysis; 2, minimum soil moisture at site; 3, *Vivoni et al.* [2008b] for site data; 4, calibration on the basis of soil moisture data comparison; 5, *Abu-Hamdeh* [2001]; 6, *Hillel* [1998]; 7, soil pit observations at site; 8, MODIS 1 km coincident data at site; 9, *Yépez et al.* [2008], on the basis of site data; 10, calibration on the basis of solar radiation data comparison; 11, calibration based on latent heat flux data comparison.

floodplain area in the domain. We selected $z_r = 1$ m, resulting in a horizontal point density ($d = 0.31$ or 31% of the DEM nodes). This selection ensures minimal model sensitivity to the TIN resolution [*Vivoni et al.*, 2005] and allows a feasible computational domain (34,302 nodes). In the resulting TIN (Figure 3a), Voronoi polygons represent a range of elevations, slopes, aspects, and contributing areas. Each polygon was assigned vegetation and soil texture properties on the basis of the dominant class within its boundaries. Five soil classes (% area): (1) sand (24.6%), (2) loamy sand (36.3%), (3) sandy loam (24.7%), (4) sandy clay loam (5.5%), and (5) rock (9.0%); and four vegetation types: (1) subtropical scrubland (75.7%), (2) oak savanna (22.3%), (3) grassland (0.9%), and (4) evergreen forest (0.9%) were used to characterize the basin (Figures 3b and 3c). A spatially uniform soil depth of 1.5 m was assumed in the basin on the basis of measurements in a set of 15 soil pits excavated in basin. Three internal subbasins, Upper (1.05 km^2), Middle (1.61 km^2), and Lower (1.05 km^2), were extracted to encompass the soil moisture sampling plots (Figure 3).

[21] The availability of model forcing and testing data at the EC site was considerably higher than in the SLL basin. We forced the point-scale simulations with EC site precipitation, incoming solar radiation, air temperature, specific humidity, and wind speed data at 30 min intervals. Model test data included radiation and energy balance components and soil moisture and soil temperature at 5, 10, and 15 cm. The EC data allow careful analysis of the simulations by inspecting multiple hydrologic processes. In contrast, the SLL basin lacked atmospheric data to force the model in a distributed fashion. As a result, meteorological data from the EC site was assumed valid in the SLL basin (~22 km distant and at higher altitude). An adiabatic temperature lapse rate (−6.5°C/km) was applied to mimic cooler basin conditions. Precipitation from stations 133 (642 m), 132 (905 m), and 146 (1375 m) were used to force the model using a Thiessen interpolation. The stations help capture to some extent the precipitation spatial variability and its elevation dependence. Testing data in the SLL basin consisted of soil moisture and temperature observations at stations 132 and 146 and the distributed soil moisture from the sampling plots.

[22] Land surface characteristics were used to parameterize the distributed model. Initial parameter estimates were obtained from field measurements of soil and vegetation properties at the site as well as remotely sensed observations [*Watts et al.*, 2007; *Vivoni et al.*, 2008b; *Yépez et al.*, 2008]. For example, albedo and surface emissivity were estimated from coincident MODIS data. Manual calibration was undertaken primarily at the EC site for the sandy loam, subtropical scrubland conditions on the basis of soil moisture and energy fluxes. Table 1 presents model parameter values used in the simulations, along with a description of sources and calibration efforts. Model parameters at the EC site were then transferred to the SLL basin with tuning of a limited number of parameters to reflect different soil and vegetation types. These minor adjustments were guided by field observations and analysis, where available, or on the basis of literature values for specific soil and vegetation classes [*Rutter et al.*, 1971; *Shuttleworth*, 1979; *Rawls et al.*, 1983; *Descroix et al.*, 2002b; *Mitchell et al.*, 2004; *Yilmaz et al.*, 2008]. This approach retains important differences in the spatial distribution of the parameters within the modeling domain. Parameter values for the distributed simulations are presented in Table 2. The initial conditions were specified as dry with negligible soil moisture above the impermeable bottom. While the lack of detailed data in the SLL basin limits potential model testing, the distributed nature of the soil moisture data set provides a strong constraint on the model capabilities.

3. Results

3.1. Soil Moisture and Energy Flux Comparisons at EC Site

[23] Point-scale simulations at the EC site were compared with soil moisture and energy flux observations during

Table 2. Model Parameters for the Major Soil and Vegetation Classes in the SLL Basin

	Major Soil Types				
Soil Properties	Sandy Loam	Loamy Sand	Sand	Sandy Clay Loam	Rock
Area (%)	24.71	36.27	24.56	5.52	8.95
K_s (mm/hr)	24.16	59.80	166.20	9.83	2.50
n	0.45	0.44	0.44	0.40	0.39
θ_s	0.41	0.40	0.42	0.33	0.39
θ_r	0.025	0.015	0.020	0.068	0.009
θ^*	0.18	0.18	0.19	0.15	0.17
m	1.50	0.45	0.60	0.32	0.16
	Major Vegetation Types				
Vegetation Properties	Subtropical Scrubland	Oak Savanna	Evergreen Forest	Grassland	
Area (%)	75.66	22.27	0.93	0.89	
v	0.60	0.45	0.65	0.30	
a	0.16	0.14	0.13	0.17	
h (m)	6.0	10.0	10.0	1.0	
K_t	0.95	0.80	0.60	0.90	
r_{min} (s/m)	20	70	85	50	

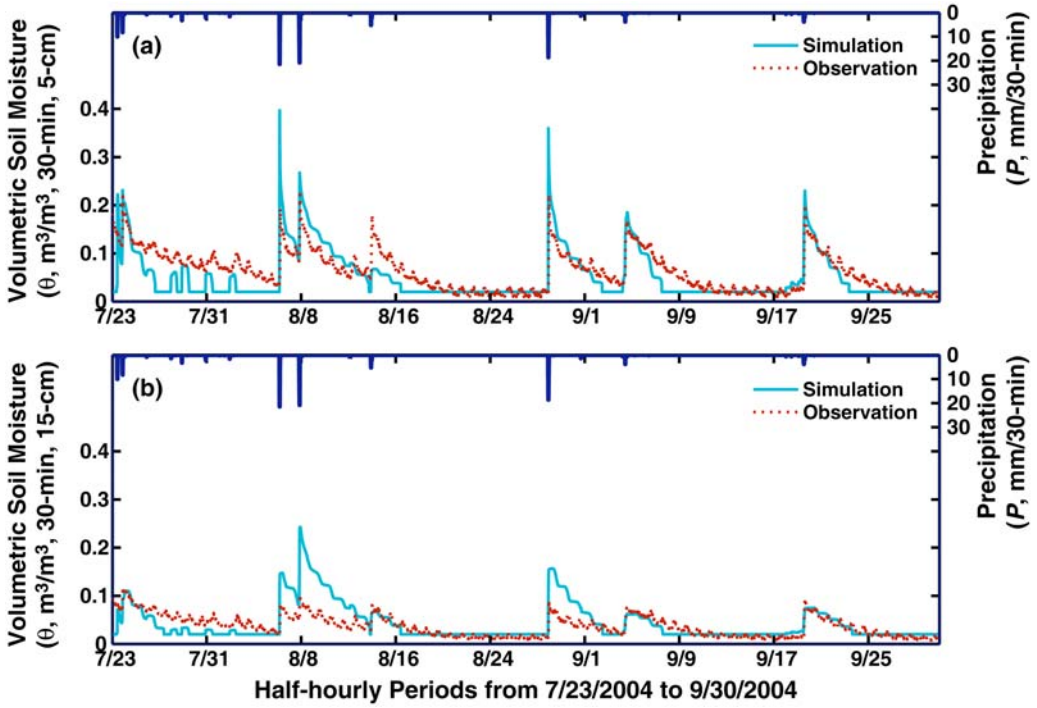

Figure 4. Comparisons of observed and simulated volumetric soil moisture (θ in m^3/m^3) at the EC site. (a) Surface soil moisture at 5 cm depth. (b) Top layer soil moisture at 15 cm depth. Data from a single sensor used in Figure 4a, while a weighted average of three sensors used in Figure 4b.

23 July to 30 September, 2004. Figure 4 presents the surface (top 5 cm, θ_{sur}) and top layer (top 15 cm, θ_{top}) soil moisture comparison. Note the good match between the simulations and observations with respect to the wetting and drying sequence. The observed peak soil moisture is overestimated during brief periods, while the recession rates are too high during the early portions of the simulation. The model match improves with time with excellent correspondence for events in September at both sampling depths. Improvements occur in soil moisture peak values and recession characteristics. This indicates that inaccuracies in the assumed dry initial condition ($\theta_i \approx \theta_r = 0.02$ m^3/m^3) were dissipated or reduced during the simulation. Quantitative soil moisture comparisons are presented in Table 3 using the bias, mean absolute error (MAE), and correlation coefficient (CC). The low MAE (0.02 m^3/m^3) and high CC (>0.65) indicate the good match between observations and simulations. A low bias for θ_{sur} and a high bias for θ_{top} also suggest the underestimation in the surface layer is because of an initial overestimation of vertical transport (i.e., infiltration) into the top layer, which is subsequently dissipated in the simulation. Overall model performance, however, is considered to be reliable at the point-scale in terms of the soil moisture response to precipitation.

[24] Figure 5 displays comparisons of observed and simulated sensible (H) and latent (λE) heat fluxes, along with the incoming solar radiation (W/m^2). Note the temporal variation of solar radiation, with large interruptions during cloudy days associated with rainfall. Several nocturnal storms, common during the NAM [e.g., *Gebremichael et al.*, 2007], have large rainfall intensities (8 August 2004). This suggests that several peak soil moisture values occur at night, leading to high plant water availability in the subsequent day. The surface flux response to wetting and drying periods is simulated well, with increases in H and decreases in λE as interstorm length increases. Rapid changes in surface fluxes during cloudy or rainy days are

Table 3. Performance Metrics Between Observed and Simulated Variables at Different Sites During Overlapping Periods[a]

	Metric		
	Bias	MAE	CC
	EC Site		
θ_{sur} (m^3/m^3)	0.82	0.02	0.76
θ_{top} (m^3/m^3)	1.16	0.02	0.65
H (W/m^2)	0.92	43.29	0.86
λE (W/m^2)	0.93	32.33	0.74
	Station 132		
θ_{sur} (m^3/m^3)	1.35	0.03	0.65
T_s (°C)	0.92	3.86	0.93
	Station 146		
θ_{sur} (m^3/m^3)	0.95	0.02	0.91
T_s (°C)	0.98	2.55	0.91
	Transect Sites		
Site 1 θ_{sur} (m^3/m^3)	0.88	0.02	0.86
Site 2 θ_{sur} (m^3/m^3)	0.68	0.04	0.95
Site 3 θ_{sur} (m^3/m^3)	0.59	0.05	0.93
Site 4 θ_{sur} (m^3/m^3)	0.70	0.03	0.79
Site 5 θ_{sur} (m^3/m^3)	0.83	0.03	0.96
Site 11 θ_{sur} (m^3/m^3)	1.13	0.02	−0.24
Site 12 θ_{sur} (m^3/m^3)	1.43	0.02	0.23
Site 13 θ_{sur} (m^3/m^3)	1.70	0.04	−0.21
Site 14 θ_{sur} (m^3/m^3)	1.06	0.01	0.27
Site 15 θ_{sur} (m^3/m^3)	1.00	0.02	0.43

[a]Bias, mean absolute error (MAE), and correlation coefficient (CC) are defined by *Vivoni et al.* [2006]. For clarity, bias is the ratio of the mean of the simulations divided by the mean of the observations. A perfect simulation has bias equal to 1, with overestimation (underestimation) having a bias greater (less) than 1.

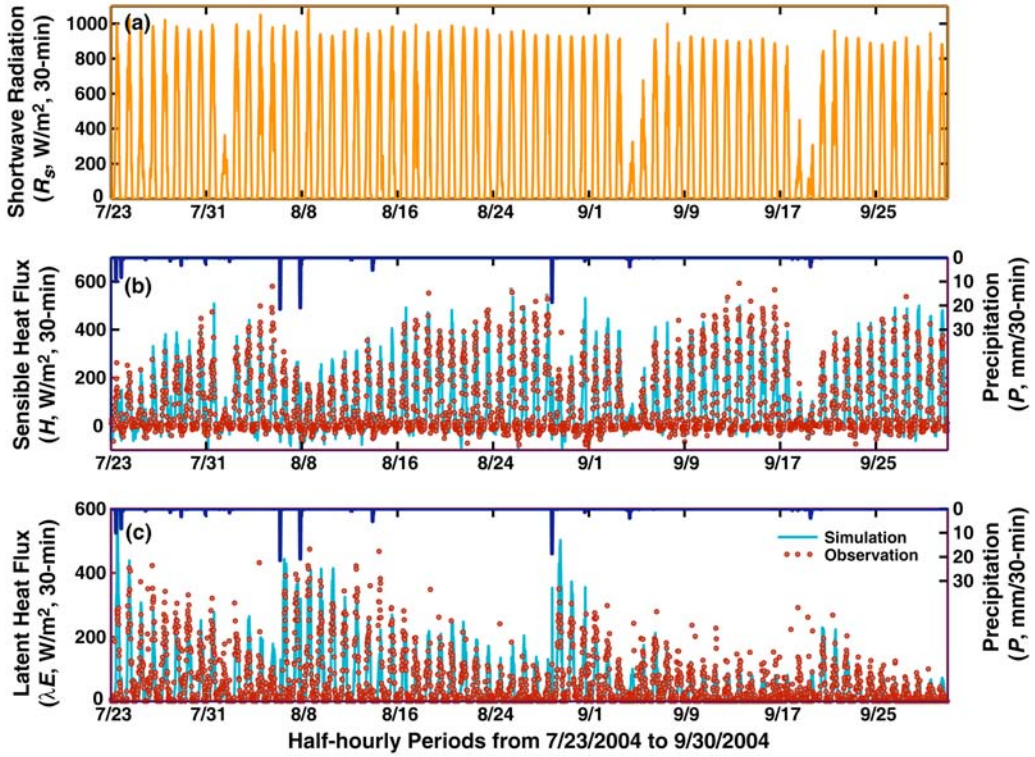

Figure 5. Comparisons of observed and simulated heat fluxes (in W/m^2). (a) Observed incoming shortwave radiation (R_s). (b) Sensible heat flux (H). (c) Latent heat flux (λE).

also captured. This behavior is confirmed by adequately simulating the temporal variation of EF (not shown). Nevertheless, there are specific periods of overestimation or underestimation of the surface fluxes, with larger discrepancies for λE. For example, from 9 to 17 September 2004, λE is underestimated, while θ_{sur} and θ_{top} are matched well, suggesting that plants may be tapping into soil moisture storage in deeper soil layers (>15 cm). Since these discrepancies are limited in time, the overall performance is characterized by a bias greater than 0.9, low MAE (<44 W/m^2), and high CC (>0.70) (Table 3). This suggests the simulations are yielding reliable soil moisture and surface fluxes, in terms of the bias, MAE, and CC metrics, for conditions after the full canopy develops.

[25] Simulation performance was also assessed in Figure 6 through the relation between daily evapotranspiration (ET) and surface soil moisture (θ) for observations, simulations, and the North American Regional Reanalysis (NARR) product [*Mesinger et al.*, 2006]. NARR consists of the corresponding variables at the colocated (32 km) pixel with the EC site [*Vivoni et al.*, 2008b]. In addition to the daily data, Figure 6 also includes piecewise linear regressions obtained for the ET-θ relation of *Rodríguez-Iturbe and Porporato* [2004]. In this relation, ET assumes stressed values above the plant wilting point (θ_w) and below a plant stress threshold (θ*), while unstressed (or maximum) ET (ET$_{max}$) occurs above θ*. The regressions allow extraction of the ET-θ relation parameters (see *Vivoni et al.* [2008b] for details). Note the excellent match between the observed and simulated ET-θ relations, including a similar range of ET and θ values. The regressions parameters (Table 4) also indicate the simulations capture well the stressed evapotranspiration (ET between θ_w and θ*) and unstressed evapotranspiration (ET$_{max}$ for $\theta > \theta$*). NARR, on the other hand, has a limited ET range, a positive bias in soil moisture, and a lack of definable stressed and unstressed ET regions, suggesting its parameterizations do not adequately represent

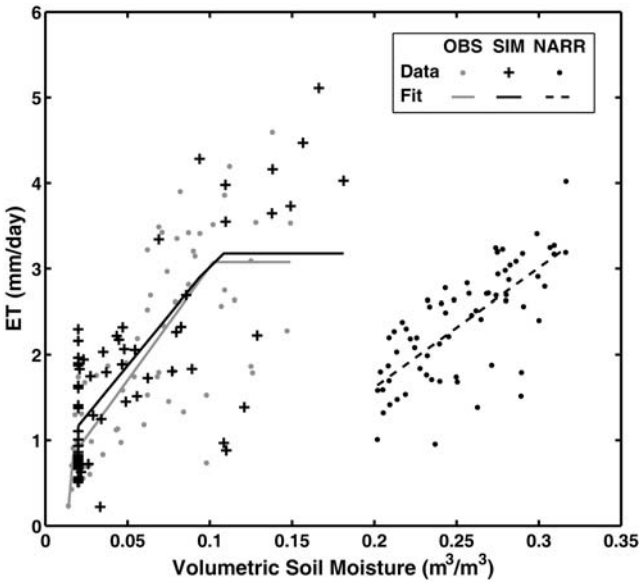

Figure 6. Comparison of daily relation between evapotranspiration and surface volumetric soil moisture for observations (OBS), model simulations (SIM), and the North American Regional Reanalysis (NARR) product. Daily values are shown as symbols, while the lines represent piecewise linear regressions as given by *Vivoni et al.* [2008b].

Table 4. Parameters of the ET-θ Relation at the Point Scale and Catchment Scale[a]

Data Set	θ_w (m^3/m^3)	θ^* (m^3/m^3)	ET_{max} (mm/d)
Point scale			
OBS	0.02	0.10	3.08
SIM	0.01	0.11	3.18
NARR	0.15	0.32	3.25
Catchment scale			
SIM	0.02	0.12	2.76

[a]OBS, observations; SIM, simulations (point scale) or basin-averaged simulations (catchment scale); NARR, North American Regional Reanalysis.

site conditions. Identified errors in the NARR ET-θ relation are not due to inaccuracies in precipitation, as the NARR rainfall during the simulation period (176 mm) is comparable to rain gauge observations (181 mm at station 132, 196 mm at station 146).

3.2. Comparison of Distributed Soil Moisture in Mountain Basin

[26] Catchment-scale simulations were compared to soil moisture and temperature data at two stations and to daily soil moisture data from sampling plots. Figure 7 compares soil moisture (θ_{sur}) and temperature (T_s) at 5 cm for stations 146 (oak savanna, loamy sand, 1375 m) and 132 (subtropical scrubland, sandy loam, 905 m). Note the varying rainfall properties at the stations and its effects on soil conditions. Model performance at station 146 is excellent, capturing the peak soil moisture values and their recessions. In addition, diurnal temperature variability and its response to cloudy conditions are consistent in the simulations, despite using solar radiation forcing from the EC site. The temperature lapse rate allowed lower soil temperatures at the high elevation site to be reproduced. Simulations at station 132, however, are not as encouraging. In particular, several rapid increases in soil moisture are not captured and the temperature is slightly underestimated. The mismatch in soil moisture is possibly due to (1) errors in the observation, as some peaks are not associated with rain, or (2) very shallow or rocky soils with low soil moisture storage capacity not captured in the simulations. Differences in the model behavior are shown quantitatively in Table 3, indicating a higher MAE, lower CC, and a bias further from unity at station 132.

[27] Reliable distributed model behavior can be further assessed through tests against the soil moisture data at the sampling plots [*Vivoni et al.*, 2007b]. Figure 8 presents the comparison at 10 sites in the Upper (sites 1–5) and Middle (sites 11–15) subbasins during a dry-down period. Sites have slightly varying soil moisture responses because of differences in meteorological forcing as well as in soil, terrain, and vegetation properties. Spatial variations in the simulated soil moisture are shown to depict georeferencing uncertainties in the observation locations and the model

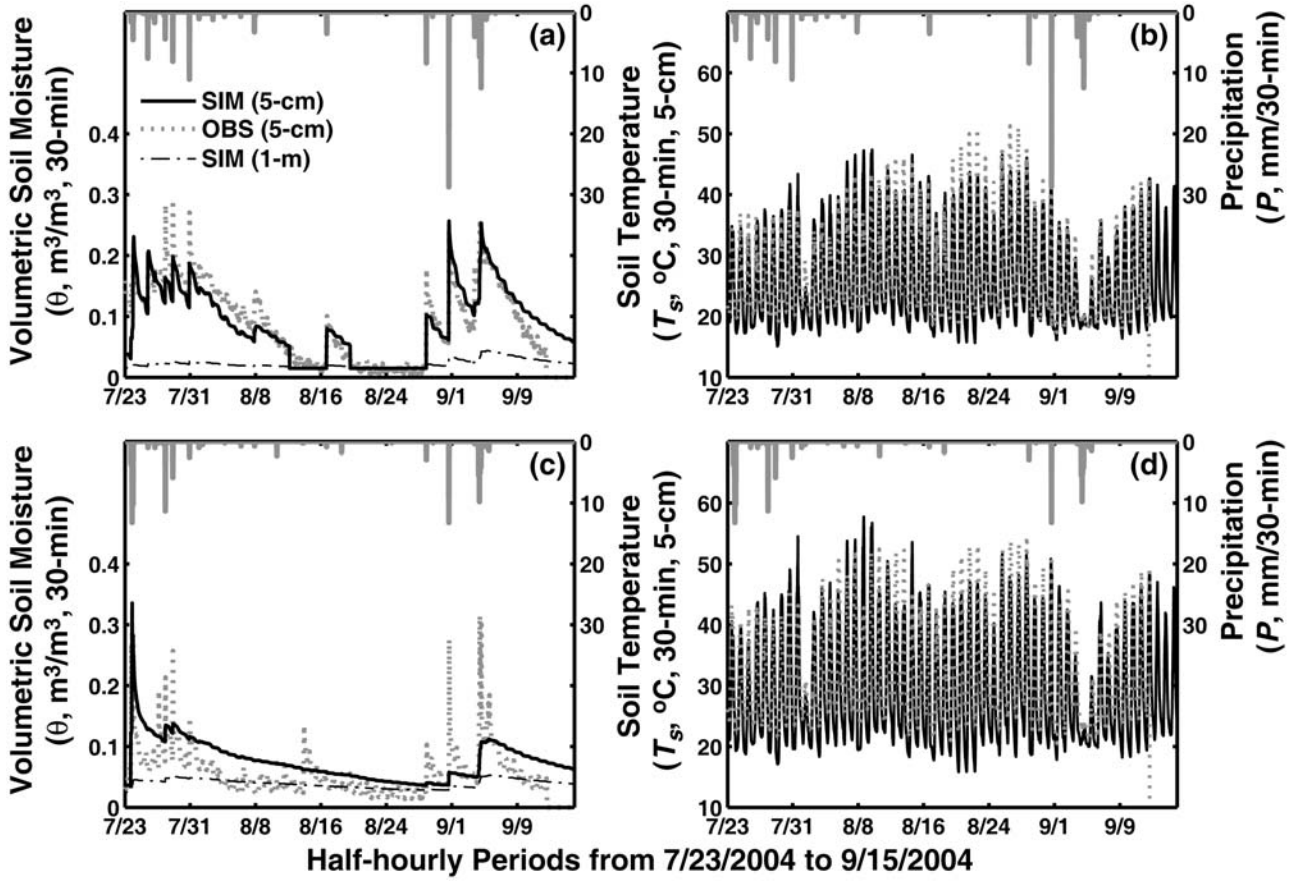

Figure 7. Comparison of observed (OBS) and simulated (SIM) volumetric soil moisture (θ in m^3/m^3) and soil temperature (T_s in °C) at SLL stations (a, b) 146 and (c, d) 132. Observed and simulated variables are at 5 cm depth. Simulated soil moisture averaged over top 1 m is also shown.

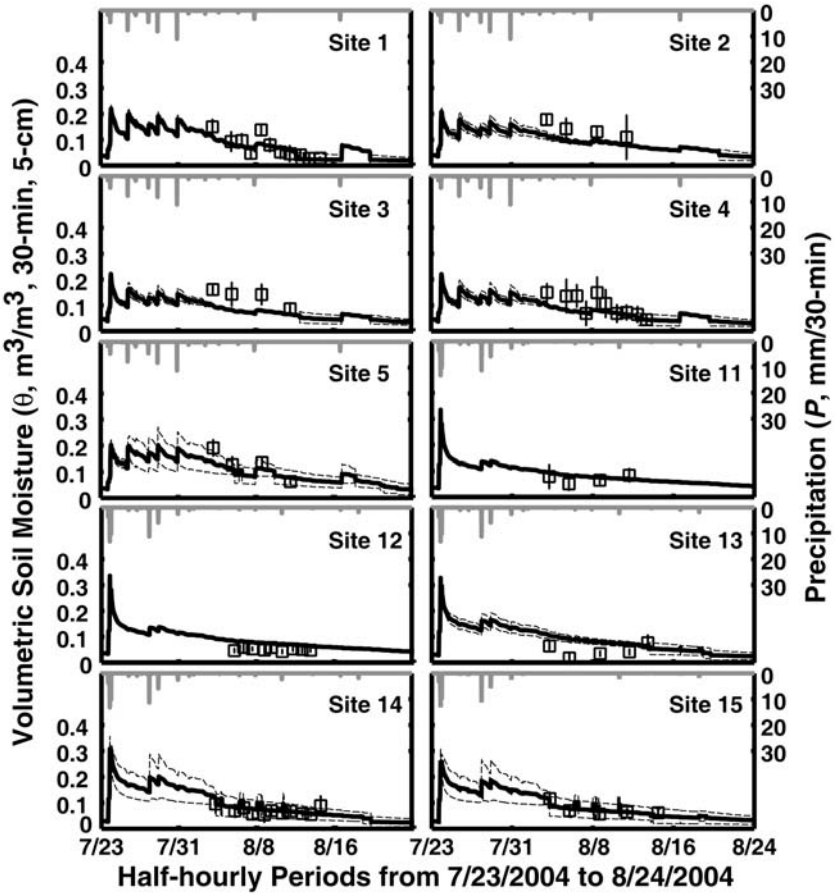

Figure 8. Distributed comparison of observed and simulated volumetric soil moisture in the SLL basin: sites 1–5 (Upper subbasin) and sites 11–15 (Middle subbasin), arranged from high to low elevation (1371–845 m). Transect observations are depicted as plot averages (squares) and ±1 SD (bars). Simulations shown as the spatial average of the colocated Voronoi polygon and its neighbors (solid lines) and ±1 SD (dashed lines).

domain representation. Overall, the distributed model provides reliable and consistent soil moisture simulations at the transect sites, including (1) capturing the overall dry-down behavior and responding to small rainfall events during the 2 week period, (2) overlapping most (but not all) of the observations within the respective uncertainty bounds at all sampling sites, and (3) matching observations consistently at a range of sites (e.g., sites 1, 5, 11, 14, and 15). At certain locations, overestimation (site 12) or underestimation (site 3) occur, though the error magnitudes (MAE) are small (Table 3). Averaged over all sites, model performance is characterized by low MAE (0.03 m^3/m^3) and a bias close to unity, indicating adequate behavior over the elevation transect.

[28] The spatial arrangement of the sampling plots allows inspection of the soil moisture variations with elevation. Figure 9 compares the distributed simulations with the colocated ground and PSR/CX soil moisture estimates. Two sampling days were selected for illustration purposes: (1) a wet day (day of year (DOY) 218) after a series of storms and (2) a dry day (DOY 226) in an interstorm period. Note the good match between the simulations and transect data for both sampling dates. In particular, the mean exhibits reasonable variations with elevation while the uncertainty bounds capture the majority of the sampling sites. Simulated spatial variability is more pronounced for the wet day, with high θ at high elevations, low θ at intermediate heights, and variable θ at low elevations, following ground data. The model also correctly reduces the spatial soil moisture variations during the dry day. Differences between the ground and PSR/CX data are pronounced for wet conditions (Figure 3d) but are smaller for the dry day where PSR/CX values are closer to the simulated range. Discrepancies between the PSR/CX and ground data for wet periods were also highlighted by *Vivoni et al.* [2008a], who suggested that potential errors may exist in the soil moisture retrieval algorithm. This suggests the various estimates converge during uniform dry conditions, but only the simulations capture the observed elevation controls during wet days.

3.3. Spatiotemporal Soil Moisture and Evapotranspiration Variability and Its Controls

[29] Given consistent performance with respect to the distributed data, we explored the spatiotemporal organization of soil moisture and evapotranspiration in the basin. Figure 10 presents basin-averaged hydrologic fluxes and states as well as the time-averaged spatial patterns. Basin-averaged variables in Figures 10a and 10c consist of mean areal precipitation (P), surface soil moisture (θ_{sur}), root zone soil moisture (θ_{rz}), evapotranspiration (ET), and surface

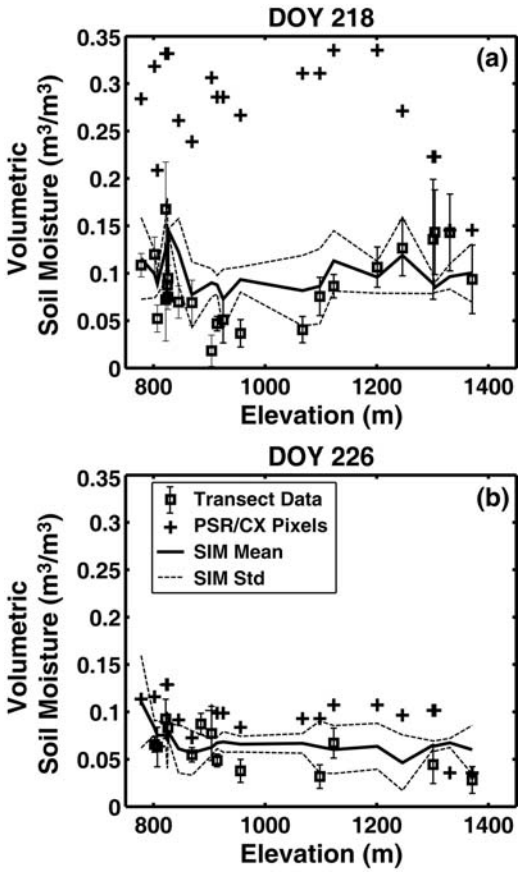

Figure 9. Comparison of ground, remotely sensed, and simulated soil moisture as a function of elevation (m) for (a) 5 August 2004 (DOY 218) and (b) 13 August 2004 (DOY 226). Ground data are plot averages, and ±1 SD (23 sites on DOY 218, 13 sites on DOY 226) is shown as squares with error bars. PSR/CX data are at the colocated 800 m pixels (crosses). Simulations are the spatial average of the colocated polygon and its neighbors (solid lines) with ±1 SD (dashed lines). All variables are the 0–5 cm soil moisture near 1200 LT. Elevations for the sampling plots are used for all products [*Vivoni et al.*, 2007b, Table 1].

runoff (Q). Note the θ_{sur} has temporal variations similar to individual sites but exhibits smoothing because of the averaging process; θ_{rz} has a modest response to rainfall, remaining fairly similar during the simulation (as in Figure 7). For comparison, the basin-averaged θ_{sur} from sampling plot and PSR/CX estimates (see *Vivoni et al.* [2008a] for aggregation details) are shown. The simulations match the transect data well, in particular for wet days in early August. PSR/CX estimates come closer to simulated values during drier days in late August. Associated with the soil moisture response are temporal changes in basin-averaged ET, with a clear decrease in ET during long interstorms and a robust increase after large rainfall events (1 September 2004). Similarly, the surface runoff at the basin outlet only occurs in response to the storm periods in July and early September.

[30] Spatial patterns in time-averaged soil moisture and evapotranspiration shown in Figures 10b and 10d are highly heterogeneous reflecting the influences of terrain, soil, vegetation properties, and meteorological forcing. Identifying specific contributions from each factor is difficult from the time-averaged patterns. Nevertheless, soil moisture differences can be discerned due to texture (Figure 3b), such as high θ in sand clay loam and low θ in exposed rock. In contrast to simulations in more humid areas [*Vivoni et al.*, 2008d], soil moisture does not appear to be well organized with distance from channels. The time-averaged ET pattern exhibits trends that follow elevation (temperature lapse rate) and precipitation (rain gauge interpolation), with higher rates at greater elevations. Overall, spatial patterns in θ and ET reflect different landscape controls, indicating the distributed behavior is much richer in complexity than the lumped response. Identifying the specific role of landscape properties is explored next using three days corresponding to wet, intermediate, and dry conditions during a long dry down (see arrows in Figures 10a and 10c). These three days were selected for illustration purposes. Results from other days within the dry-down period were verified as exhibiting similar behavior to the corresponding wetness state.

[31] Figure 11 shows surface soil moisture and evapotranspiration frequency distributions for the 3 days. Each total distribution (solid line) is further classified into soil classes to show individual contributions from each texture. The classified frequency distributions of the spatial patterns of θ and ET are effective in depicting (1) the overall decrease in θ and ET during the dry down, (2) distribution shape transitions from single modes to distinct bimodal peaks, and (3) the relative changes occurring for each soil class. Note, for example, that loamy sand sites exhibit large temporal changes as compared to sandy loam areas, indicating more rapid decreases in θ and ET. Interestingly, bimodality in θ and ET is more pronounced for the intermediate case but cannot be explained entirely from soil differences. PSR/CX data for the intermediate day (dashed line in Figure 11c) have a similar range in θ but lack the bimodality in the simulations. This suggests the intermediate case is a brief transition state exhibiting two modes: (1) a dry group where ET is nearly zero and (2) a group that sustains ET at a slightly higher θ. Under continued drying, the distribution resembles the dry group until a subsequent storm resets θ and ET to higher values.

[32] A more in-depth analysis of the landscape controls for the three days is presented in Figure 12. Catchment sites are classified using elevation, soil, and vegetation properties. For clarity, only the major soil and vegetation classes are used as these occupy 86% and 98% of the basin, respectively. As in Figure 11, the dry-down period leads to an overall reduction in θ and ET from the wet to dry days. The elevation variation, however, clearly shows (1) an overall increase (decrease) in θ and ET with elevation for wet (intermediate) states and (2) no elevation dependence of θ and ET for the dry case. These differences are prompted by variations in precipitation and temperature with elevation. Separation into soil and vegetation classes also distinguishes differences among types. Note, for example, subtropical scrubland have higher θ and lower ET than oak savannas (OAK) on loamy sand, except for the dry case where uniformity occurs. In addition, differences in θ and ET among the soils appear to be strongest for the wet case, primarily due to porosity. The pronounced bimodality for intermediate conditions (Figure 11) is partly because of differences between

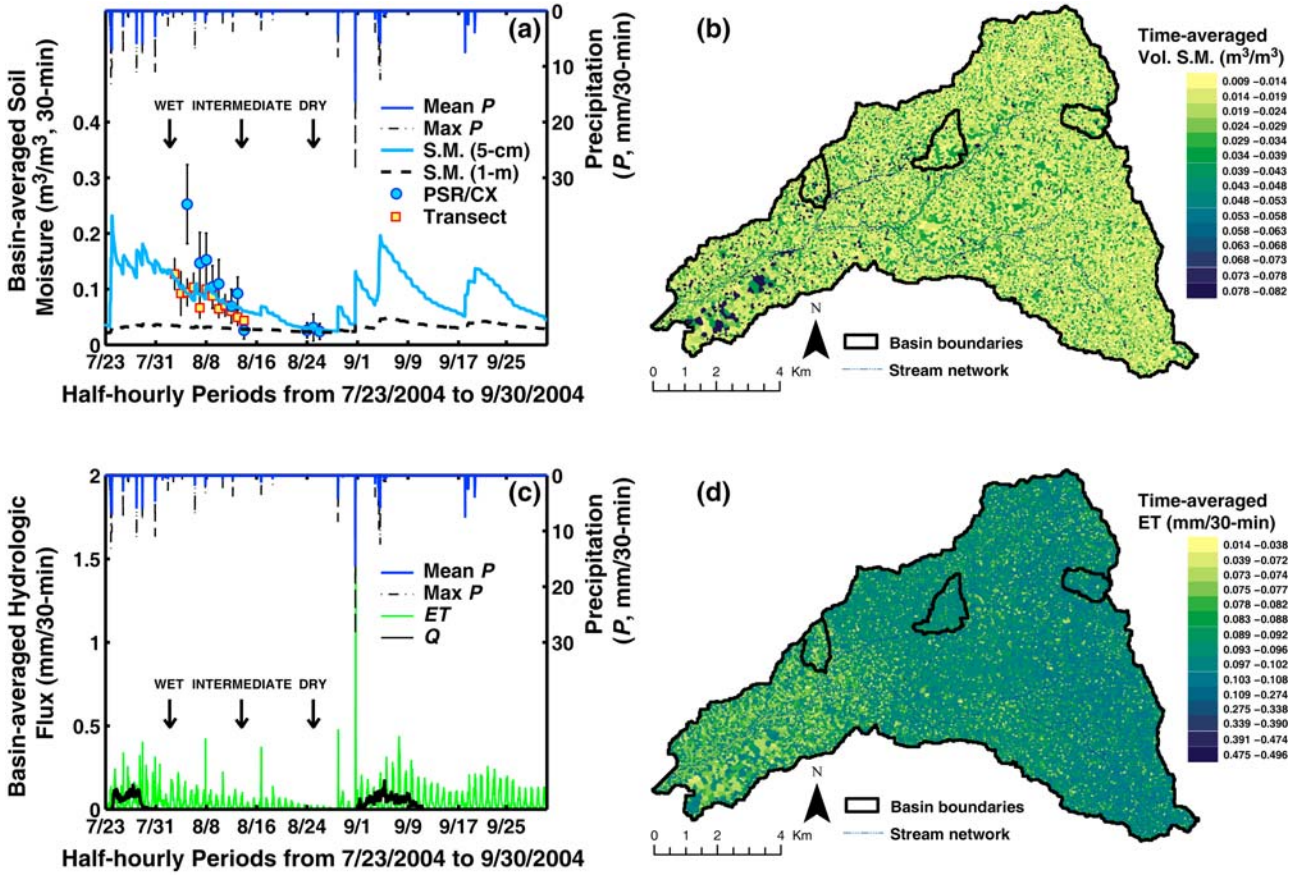

Figure 10. Simulated basin-averaged soil moisture and hydrologic fluxes. (a) Surface (5 cm) and root zone (1 m) soil moisture with mean areal (mean *P*) and maximum precipitation (max *P*). (b) Spatial distribution of time-averaged volumetric soil moisture. (c) Evapotranspiration (ET) and surface runoff (*Q*). (d) Spatial distribution of the time-averaged evapotranspiration.

subtropical scrubland (higher θ) and oak savanna (lower θ) on loamy sand at high elevations (>1000 m).

[33] The temporal evolution of the θ and ET spatial patterns are further explored in Figure 13 by inspection of the (1) basin-averaged ET-θ relation and (2) spatial variation in θ and ET as a function of the mean conditions. For each diagnostic measure, the temporal evolution is depicted through symbols grouped into weekly periods. Note the ET-θ relation evolves from high θ and ET (DOY 206–211) toward low θ and ET (DOY 236–241). This progression is interrupted by a series of storms (DOY 242–248, black squares) that increase θ and ET, resetting conditions to unstressed ET-θ values. Subsequently, the drying process decreases θ and ET through a slightly different path. This suggests that hysteresis exists in the catchment ET-θ relation induced by the temporal evolution of the complex patterns that underlie the spatially averaged conditions (note the arrows aid in tracking the temporal evolution). It is also important to note that the catchment- and point-scale ET-θ relations do not match (Table 4). While θ_w and θ^* are similar, the basin-averaged ET_{max} is significantly lower, suggesting that the distribution of soil, terrain, and vegetation properties in the catchment impacts the aggregation (or upscaling) of the ET-θ relation from point ($\sim$100 m^2) to regional ($\sim$100 km^2) scales.

[34] A hysteresis loop is also observed in the evolution of the spatial standard deviation of θ (σ_θ) with respect to the mean soil moisture (μ_θ). Arrows in Figure 13b aid in tracking the progression of the $\sigma_\theta - \mu_\theta$ relation from wet states with high spatial variability (DOY 206–211) to dry conditions with low variations (DOY 236–241). Note the $\sigma_\theta - \mu_\theta$ relation is linear at high and low θ, following the pooled PSR/CX and transect data [*Vivoni et al.*, 2008a]. In the interval ($0.05 < \theta < 0.1$ m^3/m^3), σ_θ varies nonlinearly with μ_θ, exhibiting lower values than observed. This interval corresponds to the intermediate case, suggesting that the strong bimodality reduces the spatial variation. The drying and homogenization pathway is interrupted by storm events (DOY 242–248), which increase both σ_θ and μ_θ, likely because of the spatial variation in precipitation. Upon further drying, the $\sigma_\theta - \mu_\theta$ relation is reestablished along a slightly different path. Interestingly, convergence is observed in the dry-down arm of the hysteresis loop within the intermediate interval. The simulated temporal evolution is expected to continue in a cyclic fashion prompted by intense, spatially variable precipitation and prolonged drying periods.

[35] An analogous temporal evolution occurs for the spatial variability of ET (σ_{ET}) with the mean ET (μ_{ET}). The hysteresis loop, however, is not as pronounced (or open) and exhibits a linear $\sigma_{ET} - \mu_{ET}$ relation ($\sigma_{ET} = 0.19\mu_{ET} + 0.17$, $R^2 = 0.91$, not shown), when the strong rainfall periods (DOY 242–248) are excluded. Pronounced, spatially variable precipitation events lead to large increases

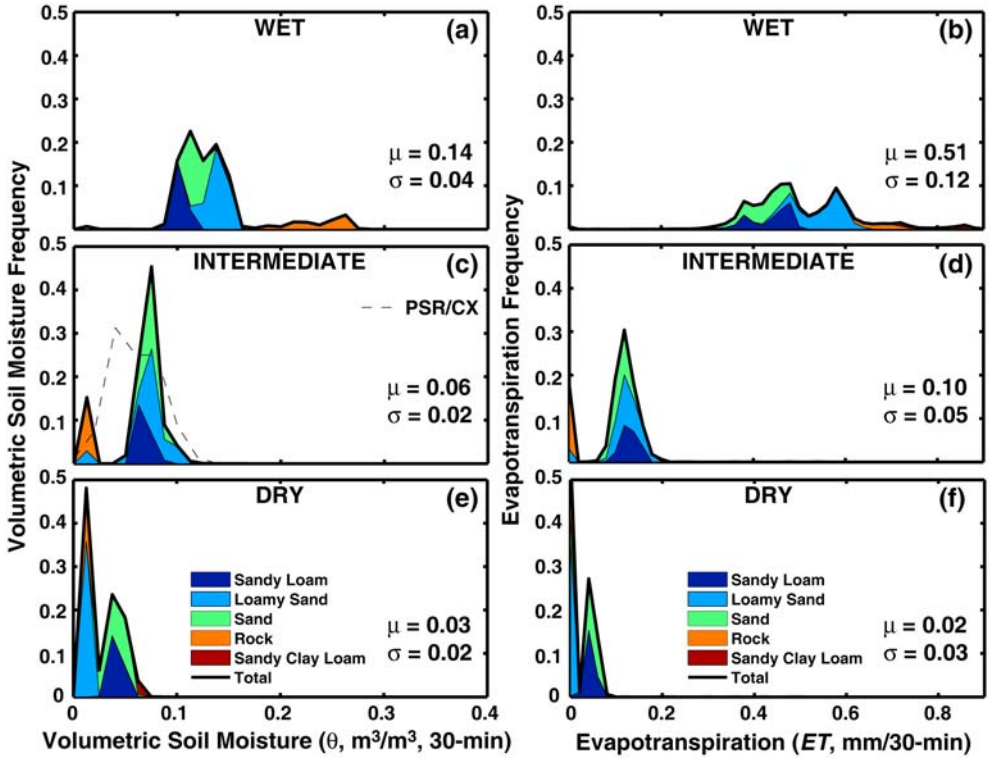

Figure 11. Temporal evolution of soil moisture and evapotranspiration frequency distributions for (a, b) wet, (c, d) intermediate, and (e, f) dry conditions at the catchment scale (N = 34,302). Conditions correspond to DOY 215 (2 August 2004), DOY 226 (13 August 2004), and DOY 237 (24 August 2004) at 1200 LT. The spatial mean (μ) and standard deviation (σ) are shown. Frequency bin widths are 0.0125 m^3/m^3 and 0.02 mm/30 min for θ and ET, respectively.

in σ_{ET}, through soil moisture variability, that are on the order of μ_{ET} (~2 mm/d). Nevertheless, spatial ET variations are rapidly dissipated by the landscape conditions, collapsing back to the linear relation. The monotonically increasing form of the $\sigma_{ET} - \mu_{ET}$ relation indicates that ET variability in a catchment may be readily estimated from remotely sensed observations or modeling of basin-averaged conditions during the majority of conditions.

4. Discussion

4.1. Internal Evaluation and Applications of Hydrologic Models in Complex Basins

[36] Distributed evaluation of hydrologic models is challenging in any setting but can be considerably more difficult in semiarid mountain catchments because of (1) the discontinuous nature of the catchment soil moisture and subsurface saturation [*Maneta et al.*, 2008], (2) the strong role played by patchy antecedent wetness on the basin response [*Wooldridge et al.*, 2003], and (3) the direct link between evapotranspiration and soil moisture in water-limited settings [*Vivoni et al.*, 2008b]. A few studies have tested distributed models in semiarid basins through verification at multiple sites [*Maneta et al.*, 2008; *Loiza Usuga and Pauwels*, 2008; *Mahmood and Vivoni*, 2008]. Greater progress in testing distributed soil moisture simulations has been made in humid areas [*Western and Grayson*, 2000], where terrain-mediated redistribution has a strong control on spatial patterns. Even in humid basins, however, soil moisture can exhibit discontinuous patterns during interstorm periods that have high evapotranspiration demand [*Western et al.*, 1999].

[37] The point- and catchment-scale evaluations performed in this study indicate a reliable and consistent model performance in relation to the SMEX04-NAME data sets [e.g., *Watts et al.*, 2007; *Vivoni et al.*, 2007b, 2008a]. Matching the multiple hydrologic observations at the EC site provided confidence to apply the model to the mountain basin despite the more limited data sets. While the modeling domains share the same major ecosystem, the SLL basin has a large range of soil and terrain conditions. Distributed model evaluations reveal that the observed soil moisture evolution is captured in lumped and distributed fashions. More importantly, wet periods exhibit elevation dependence in soil moisture spatial patterns, while dry states are spatially uniform in the simulations. This suggests that terrain controls on soil moisture can be simulated in semiarid mountain basins, in a fashion similar to that of *Western and Grayson* [2000] for more humid settings. Clearly, obtaining accurate spatial observations that are commensurate with the complex basin characteristics would allow a more thorough testing of the simulated hydrologic processes.

[38] Distributed model evaluations with respect to the aircraft-based data and the NARR product also yield insight into the value of high-resolution simulations in complex basins. The simulated spatiotemporal patterns could help

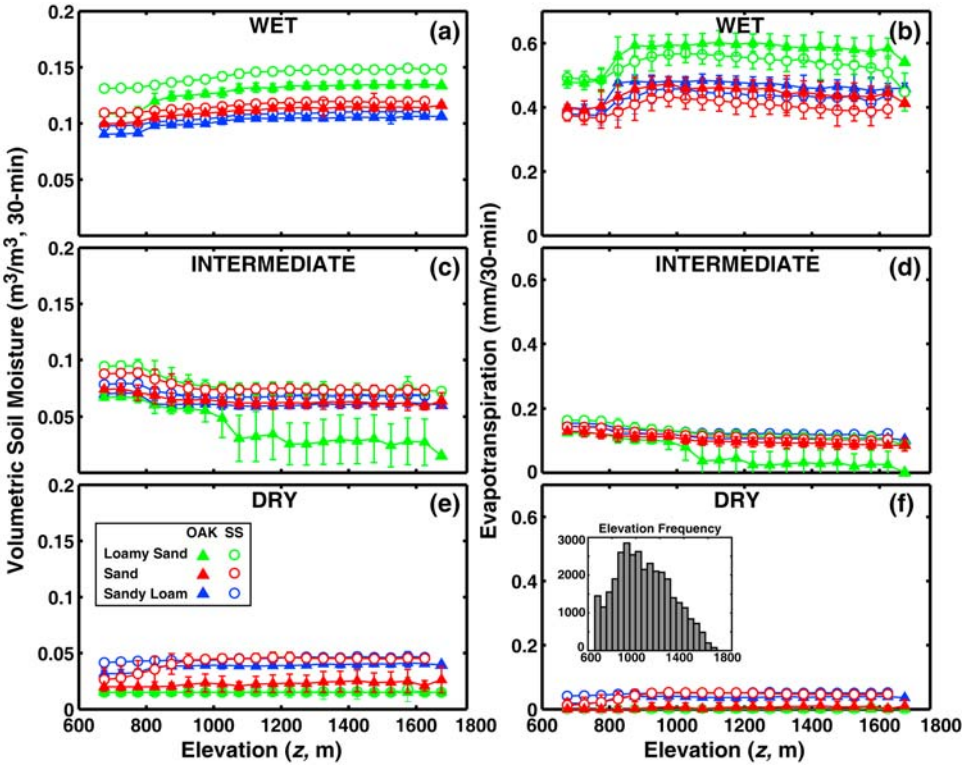

Figure 12. Temporal evolution of landscape controls on soil moisture and evapotranspiration for (a, b) wet, (c, d) intermediate, and (e, f) dry conditions. Landscape controls are captured through classifications by elevation, soil, and vegetation. Symbols represent bin averages, while error bars depict ±1 SD for elevation bin widths of 50 m. The elevation frequency (inset in Figure 12f) indicates the number of sites per elevation bin.

improve the retrieval of soil moisture from PSR/CX brightness temperature fields [*Bindlish et al.*, 2008] by providing a bias correction, in particular for wet conditions. Aggregation of the simulated fields to PSR/CX (800 m) resolution can also help quantify the subgrid pixel variability (e.g., $\sigma_\theta - \mu_\theta$ relation) and its variation with catchment properties [*Jacobs et al.*, 2004; *Famiglietti et al.*, 2008]. The simulated ET-θ relation also reveals that improvements are feasible to the NARR product [*Mesinger et al.*, 2006] by parameterizing the underlying land surface model specifically for northwest Mexico. More importantly, the ET-θ relation exhibits scale dependence in ET_{max} as catchment patterns are aggregated from the point scale. Thus, comparisons between point and coarse regional products should be performed with care where aggregation is complicated by landscape heterogeneity [cf. *Crow and Wood*, 2002].

4.2. Identifying Catchment Controls on Soil Moisture and Evapotranspiration Patterns

[39] Catchment processes and their spatial organization are known to vary across climate zones through the control exerted by the mean wetness state [e.g., *Sivapalan*, 2005; *Teuling and Troch*, 2005; *Lawrence and Hornberger*, 2007; *Vivoni et al.*, 2007a]. Catchment simulations allow a rough assessment of the seasonal water balance, resulting in ET/$P \sim 0.76$ and $Q/P \sim 0.21$ with the remainder as increases in soil moisture storage. While this lumped estimate is based on basin-averaged fluxes rather than a distributed analysis, it indicates considerably higher values of Q/P as compared to annual analyses ranging from 0.02 to 0.05 in the broader NAM region [e.g., *Grimm et al.*, 1997; *Gochis et al.*, 2003]. The simulated seasonal Q/P is more comparable to observations from headwater basins in southern Sonora reported by *Gochis et al.* [2006], ranging from 0.09 to 0.19. The simulations also indicate that precipitation in the mountain basin yields streamflow and increases in basin wetness, despite the high evapotranspiration rates. As a result, the catchment conditions should be considered as "seasonally wet with prolonged dry downs," or as an alternating cycle of "humid" and "semiarid" states. This is consistent with terrain-mediated soil moisture patterns during wet periods and nearly uniform distributions during dry downs.

[40] Prolonged dry downs embedded within the NAM season also facilitate identification of the landscape controls on soil moisture and evapotranspiration spatial patterns. A useful way to synthesize the controls of soil, terrain, and vegetation properties is to consider them in light of the work by *Lawrence and Hornberger* [2007], who suggested climate dictates whether vegetation (semiarid), terrain (temperate), or soil (humid) properties determine soil moisture variability. In this study, catchment θ and ET distributions exhibit (1) large differences among soil types for the wet state, (2) important elevation differences for the wet and intermediate cases, and (3) more pronounced vegetation differences for intermediate and dry states for specific soil

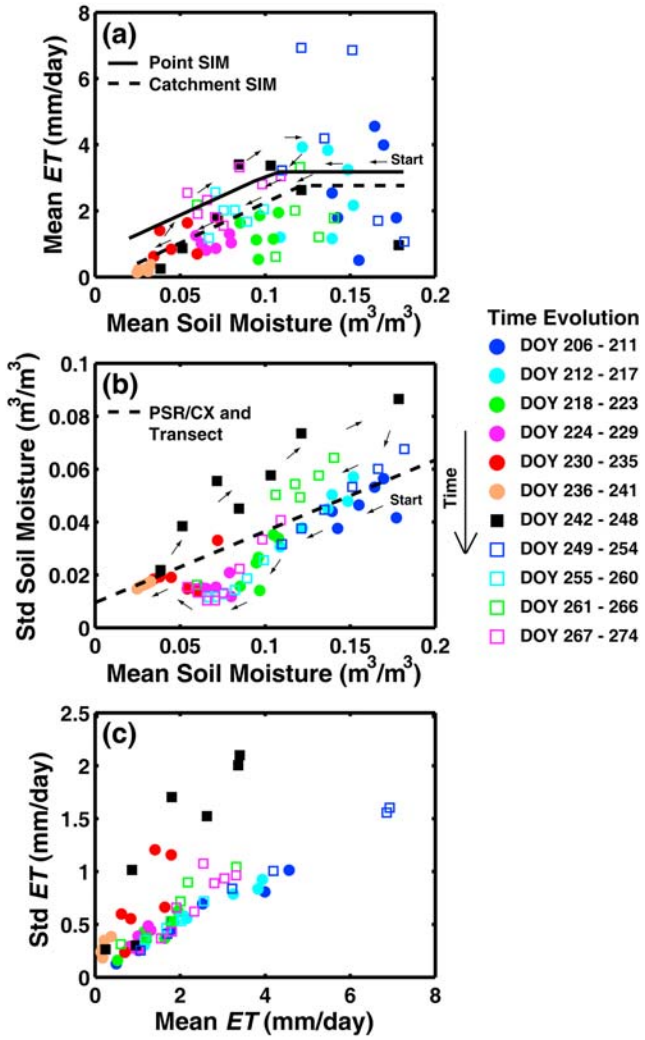

Figure 13. Temporal evolution of volumetric soil moisture and evapotranspiration conditions in the catchment. (a) Daily relation between basin-averaged ET and θ. Lines represent piecewise linear regressions for EC and catchment simulations. (b) Daily relation between spatial standard deviation in θ and basin-averaged θ. Dashed line represents relation for PSR/CX pixels and ground data. (c) Daily relation between spatial standard deviation in ET and basin-averaged ET. Note that DOY 206 is 24 July 2004 and DOY 274 is 30 September 2004.

types. Our results agree well with those *Lawrence and Hornberger* [2007], though they were obtained from a more limited range of $0.025 < \theta < 0.18$ m^3/m^3, as compared to $0.08 < \theta < 0.4$ m^3/m^3 in their study. Thus, the dominant landscape controls occur in the sequence: soil (wet), terrain (wet, intermediate), and vegetation (intermediate, dry). While the organized pattern of landscape effects is encouraging, this should be tempered by the fact that the catchment simulations exhibit high heterogeneity and differences among soil, terrain, and vegetation types occur across a wide range of conditions. The important point to be made is that landscape controls may follow a sequence according to mean wetness even within the same climate setting when seasonality allows alternating states.

4.3. Complexity and Emergent Patterns in Catchment Response

[41] Distributed hydrologic simulations depend on the model capabilities and limitations and the data sets used in catchment applications. Nevertheless, models serve as our best available representations of the real world because of inherent difficulties in observing complex basins [e.g., *Mirus et al.*, 2009]. When heterogeneous distributions are used to drive distributed models, the resulting spatiotemporal hydrologic responses are complex [e.g., *Ivanov et al.*, 2004b; *Caylor et al.*, 2005; *Bertoldi et al.*, 2006; *Vivoni et al.*, 2008d]. Despite this complexity, simple patterns may emerge. In this study, hysteresis in the temporal evolutions of the spatial variability of θ and ET can be considered as emergent patterns. These arise from the aggregation of a complex set of underlying processes responding to two types of forcing: (1) precipitation events that rapidly increase θ and ET and (2) evapotranspiration demands that diminish θ and ET over prolonged periods. The precipitation characteristics are key in determining the wetting arm of the hysteresis loop, while the landscape controls are essential in establishing a converging drying arm. It is feasible to envision hysteresis loops of different shapes or sizes depending on climate forcing and the basin properties. Clearly, asymmetry in the hysteresis arms will depend on the relative spatial variations in climate forcing that wet the basin versus land surface properties controlling the basin drying. In this study, the rainfall distribution from a limited set of rain gauges was more spatially variable than the effects of soil, vegetation, and topography on the soil moisture dry down. Similar hysteresis was observed in a small, humid setting by *Teuling et al.* [2007], suggesting this emergent behavior may exist across climate zones and scales.

5. Concluding Remarks

[42] This study explores the spatiotemporal variability in catchment-scale soil moisture and evapotranspiration patterns simulated by a distributed hydrologic model subject to in-phase precipitation and radiation forcing during the NAM. It is considered to be the most intensive and extensive attempt to date in testing a distributed model in the semiarid mountain region of northwest Mexico. By quantifying the catchment response through various diagnostic metrics, we describe the spatiotemporal evolution and identify controls of landscape properties on the simulated soil moisture and evapotranspiration fields. This modeling exercise yielded unexpected outcomes, including a strong bimodality in catchment patterns during brief transitions and hysteresis loops in the relation between spatial variability and mean states. Both outcomes are explained by the interplay of basin properties with alternating wet and dry periods during the NAM, suggesting these emergent patterns may exist elsewhere at the catchment scale.

[43] **Acknowledgments.** Funding from the Army Research Office (56059-EV-PCS), NOAA Climate Program Office (GC07-019), NSF IRES Program (OISE 0553852), USDA-ARS SMEX04 project, and U.S. Fulbright-García Robles Scholar Program to Enrique R. Vivoni is acknowledged. The authors also thank the numerous students and researchers from the United States and Mexico who participated in the field sampling and data processing, in particular Hugo Gutiérrez-Jurado, Giuseppe Mascaro, James Craft, Whitney DeFoor, J. Bruce Harrison, Hernan Moreno, Luis Méndez-Barroso, and Agustín Robles-Morua. We also thank David J.

Gochis and two anonymous reviewers for insightful comments that helped improve an early version of the manuscript.

References

Abu-Hamdeh, N. H. (2001), Measurement of the thermal conductivity of sandy loam and clay loam using single and dual probes, *J. Agric. Eng. Res.*, *80*(2), 209–216, doi:10.1006/jaer.2001.0730.

Adams, D. K., and A. C. Comrie (1997), The North American Monsoon, *Bull. Am. Meteorol. Soc.*, *78*(10), 2197–2213, doi:10.1175/1520-0477(1997)078<2197:TNAM>2.0.CO;2.

Bertoldi, G., R. Rigon, and T. M. Over (2006), Impact of watershed geomorphic characteristics on the energy and water budgets, *J. Hydrometeorol.*, *7*, 389–403, doi:10.1175/JHM500.1.

Bindlish, R., T. J. Jackson, A. J. Gasiewski, B. Stankov, M. H. Cosh, I. Mladenova, E. R. Vivoni, V. Lakshmi, C. J. Watts, and T. Keefer (2008), Aircraft-based soil moisture retrievals in mixed vegetation and topographic conditions, *Remote Sens. Environ.*, *112*(2), 375–390, doi:10.1016/j.rse.2007.01.024.

Brito-Castillo, L., A. V. Douglas, A. Leyva-Contreras, and D. Lluch-Belda (2003), The effect of large-scale circulation on precipitation and streamflow in the Gulf of California continental watershed, *Int. J. Climatol.*, *23*(7), 751–768, doi:10.1002/joc.913.

Cabral, M. C., L. Garrote, R. L. Bras, and D. Entekhabi (1992), A kinematic model of infiltration and runoff generation in layered and sloped soils, *Adv. Water Resour.*, *15*, 311–324, doi:10.1016/0309-1708(92)90017-V.

Caylor, K. K., S. Manfreda, and I. Rodríguez-Iturbe (2005), On the coupled geomorphological and ecohydrological organization of river basins, *Adv. Water Resour.*, *28*, 69–86, doi:10.1016/j.advwatres.2004.08.013.

Coblentz, D. D., and K. H. Riitters (2004), Topographic controls on the regional-scale biodiversity of the south-western USA, *J. Biogeogr.*, *31*(7), 1125–1138, doi:10.1111/j.1365-2699.2004.00981.x.

Cosh, M. H., T. J. Jackson, R. Bindlish, J. S. Famiglietti, and D. Ryu (2005), Calibration of an impedance probe for estimation of surface soil water content over large areas, *J. Hydrol.*, *311*, 49–58, doi:10.1016/j.jhydrol.2005.01.003.

Crave, A., and C. Gascuel-Odoux (1997), The influence of topography on time and space distribution of soil surface water content, *Hydrol. Processes*, *11*, 203–210, doi:10.1002/(SICI)1099-1085(199702)11:2<203::AID-HYP432>3.0.CO;2-K.

Crow, W. T., and E. F. Wood (2002), The value of coarse-scale soil moisture observations for regional surface energy balance modeling, *J. Hydrometeorol.*, *3*, 467–482, doi:10.1175/1525-7541(2002)003<0467:TVOCSS>2.0.CO;2.

Crow, W. T., D. Ryu, and J. S. Famiglietti (2005), Upscaling of field-scale soil moisture measurements using distributed land surface modeling, *Adv. Water Resour.*, *28*, 1–14, doi:10.1016/j.advwatres.2004.10.004.

Descroix, L., J. L. Gonzalez Barrios, J. P. Vandervaere, D. Viramontes, and A. Bollery (2002a), An experimental analysis of hydrodynamic behavior on soils and hillslopes in a subtropical mountainous environment (western Sierra Madre, Mexico), *J. Hydrol.*, *266*, 1–14, doi:10.1016/S0022-1694(02)00099-9.

Descroix, L., J.-F. Nouvelot, and M. Vauclin (2002b), Evaluation of an antecedent precipitation index to model runoff yield in the western Sierra Madre (north–west Mexico), *J. Hydrol.*, *263*, 114–130, doi:10.1016/S0022-1694(02)00047-1.

Dominguez, F., P. Kumar, and E. R. Vivoni (2008), Precipitation recycling variability and ecoclimatological stability—A study using NARR data. Part II: North American monsoon region, *J. Clim.*, *21*(20), 5187–5203, doi:10.1175/2008JCLI1760.1.

Douglas, M. W., R. A. Maddox, K. Howard, and S. Reyes (1993), The Mexican monsoon, *J. Clim.*, *6*, 1665–1677, doi:10.1175/1520-0442(1993)006<1665:TMM>2.0.CO;2.

Famiglietti, J. S., D. Ryu, A. A. Berg, M. Rodell, and T. J. Jackson (2008), Field observations of soil moisture variability across scales, *Water Resour. Res.*, *44*, W01423, doi:10.1029/2006WR005804.

Garrote, L., and R. L. Bras (1995), A distributed model for real-time flood forecasting using digital elevation models, *J. Hydrol.*, *167*, 279–306, doi:10.1016/0022-1694(94)02592-Y.

Gebremichael, M., E. R. Vivoni, C. J. Watts, and J. C. Rodriguez (2007), Sub-mesoscale spatiotemporal variability of North American monsoon rainfall over complex terrain, *J. Clim.*, *20*(9), 1751–1773, doi:10.1175/JCLI4093.1.

Gochis, D. J., W. J. Shuttleworth, and Z. L. Yang (2003), Hydrometeorological response of the modeled North American monsoon to convective parameterization, *J. Hydrometeorol.*, *4*(2), 235–250, doi:10.1175/1525-7541(2003)4<235:HROTMN>2.0.CO;2.

Gochis, D. J., A. Jiménez, C. J. Watts, J. Garatuza-Payán, and W. J. Shuttleworth (2004), Analysis of 2002 and 2003 warm-season precipitation from the North American monsoon experiment event rain gauge network, *Mon. Weather Rev.*, *132*(12), 2938–2953, doi:10.1175/MWR2838.1.

Gochis, D. J., L. Brito-Castillo, and W. J. Shuttleworth (2006), Hydroclimatology of the North American monsoon region in northwest Mexico, *J. Hydrol.*, *316*(1–4), 53–70, doi:10.1016/j.jhydrol.2005.04.021.

Goodrich, D. C., T. J. Schmugge, T. J. Jackson, C. L. Unkrich, T. O. Keefer, R. Parry, L. B. Bach, and S. A. Am (1994), Runoff simulation sensitivity to remotely sensed initial soil water content, *Water Resour. Res.*, *30*(5), 1393–1405, doi:10.1029/93WR03083.

Grayson, R. B., A. W. Western, F. H. S. Chiew, and G. Bloschl (1997), Preferred states in spatial soil moisture patterns: Local and nonlocal controls, *Water Resour. Res.*, *33*(12), 2897–2908, doi:10.1029/97WR02174.

Grayson, R. B., G. Bloschl, A. W. Western, and T. A. McMahon (2002), Advances in the use of observed spatial patterns of catchment hydrological response, *Adv. Water Resour.*, *25*, 1313–1334, doi:10.1016/S0309-1708(02)00060-X.

Grimm, N. B., A. Chacon, C. N. Dahm, S. W. Hostetler, O. T. Lind, P. L. Starkweahter, and W. W. Wurtsbaugh (1997), Sensitivity of aquatic ecosystems to climatic and anthropogenic changes: The Basin and Range, American Southwest and Mexico, *Hydrol. Processes*, *11*, 1023–1041, doi:10.1002/(SICI)1099-1085(19970630)11:8<1023::AID-HYP516>3.0.CO;2-A.

Higgins, R. W., and D. J. Gochis (2007), Synthesis of results from the North American Monsoon Experiment (NAME) process study, *J. Clim.*, *20*(9), 1601–1607, doi:10.1175/JCLI4081.1.

Higgins, R. W., et al. (2003), Progress in Pan American CLIVAR Research: The North American monsoon system, *Atmósfera*, *16*, 29–65.

Hillel, D. (1998), *Environmental Soil Physics: Fundamentals, Applications, and Environmental Considerations*, 771 pp., Academic, San Diego, Calif.

Instituto Nacional de Estadística, Geografía e Informática (INEGI) (1998), Modelos digitales de elevación, scale 1:24000, Mexico City.

Instituto Nacional de Investigaciones Forestales, Agrícolas y Pecuarias (INIFAP) (2001), Inventario Nacional de Suelos, scale 1:250,000, Mexico City.

Ivanov, V. Y., E. R. Vivoni, R. L. Bras, and D. Entekhabi (2004a), Catchment hydrologic response with a fully distributed triangulated irregular network model, *Water Resour. Res.*, *40*(11), W11102, doi:10.1029/2004WR003218.

Ivanov, V. Y., E. R. Vivoni, R. L. Bras, and D. Entekhabi (2004b), Preserving high-resolution surface and rainfall data in operational-scale basin hydrology: A fully distributed, physically based approach, *J. Hydrol.*, *298*(1–4), 80–111, doi:10.1016/j.jhydrol.2004.03.041.

Jackson, T. J., R. Bindlish, A. J. Gasiewski, B. Stankov, M. Klein, E. G. Njoku, D. Bosch, T. L. Coleman, C. A. Laymon, and P. Starks (2005), Polarimetric scanning radiometer C- and X-band microwave observations during SMEX03, *IEEE Trans. Geosci. Remote Sens.*, *43*(11), 2419–2430, doi:10.1109/TGRS.2005.857625.

Jacobs, J. M., B. P. Mohanty, E.-C. Hsu, and D. Miller (2004), SMEX02: Field scale variability, time stability and similarity of soil moisture, *Remote Sens. Environ.*, *92*, 436–446, doi:10.1016/j.rse.2004.02.017.

Kim, G., and A. Barros (2002), Space-time characterization of soil moisture from passive microwave remotely sensed imagery and ancillary data, *Remote Sens. Environ.*, *81*, 393–403, doi:10.1016/S0034-4257(02)00014-7.

Kurc, S. A., and E. E. Small (2004), Dynamics of evapotranspiration in semiarid grassland and shrubland ecosystems during the summer monsoon season, central New Mexico, *Water Resour. Res.*, *40*(9), W09305, doi:10.1029/2004WR003068.

Lawrence, J. E., and G. M. Hornberger (2007), Soil moisture variability across climate zones, *Geophys. Res. Lett.*, *34*, L20402, doi:10.1029/2007GL031382.

Loiza Usuga, J. C., and V. R. N. Pauwels (2008), Calibration and multiple data set-based validation of a land surface model in a mountainous Mediterranean study area, *J. Hydrol.*, *356*, 223–233, doi:10.1016/j.jhydrol.2008.04.018.

Maass, J. M., J. M. Vose, W. T. Swank, and A. Martínez-Yrizar (1995), Seasonal changes of leaf area index (LAI) in a tropical deciduous forest in west Mexico, *For. Ecol. Manage.*, *74*, 171–180, doi:10.1016/0378-1127(94)03485-F.

Mahmood, T. H., and E. R. Vivoni (2008), Evaluation of distributed soil moisture simulations through field observations during the North

American monsoon in Redondo Creek, New Mexico, *Ecohydrology*, *1*(3), 271–287, doi:10.1002/eco.23.

Maneta, M., S. Schnabel, and V. Jetten (2008), Continuous spatially distributed simulation of surface and subsurface hydrological processes in a small semiarid catchment, *Hydrol. Processes*, *22*, 2196–2214, doi:10.1002/hyp.6817.

Méndez-Barroso, L. A., and E. R. Vivoni (2010), Observed shifts in land surface conditions during the North American monsoon: Implications for a vegetation-rainfall feedback mechanism, *J. Arid Environ.*, doi:10.1016/j.jaridenv.2009.09.026, in press.

Méndez-Barroso, L. A., E. R. Vivoni, C. J. Watts, and J. C. Rodríguez (2009), Seasonal and interannual relations between precipitation, surface soil moisture and vegetation dynamics in the North American monsoon region, *J. Hydrol.*, *377*, 59–70, doi:10.1016/j.jhydrol.2009.08.009.

Mesinger, F., et al. (2006), North American regional reanalysis, *Bull. Am. Meteorol. Soc.*, *87*(3), 343–360, doi:10.1175/BAMS-87-3-343.

Mirus, B. B., K. Loague, J. E. VanderKwaak, S. K. Kampf, and S. J. Burges (2009), A hypothetical reality of Tarrawarra-like hydrologic response, *Hydrol. Processes*, *23*, 1093–1103, doi:10.1002/hyp.7241.

Mitchell, K. E., et al. (2004), The multi-institution North American Land Data Assimilation System (NLDAS): Utilizing multiple GCIP products and partners in a continental distributed hydrological modeling system, *J. Geophys. Res.*, *109*(D7), D07S90, doi:10.1029/2003JD003823.

Mo, K. C. (2008), Influence of sea surface temperature on soil moisture and precipitation over the southwest, *J. Geophys. Res.*, *113*, D12116, doi:10.1029/2007JD009221.

Mora, F., and L. R. Iverson (1998), On the sources of vegetation activity variation, and their relation with water balance in Mexico, *Int. J. Remote Sens.*, *19*(10), 1843–1871, doi:10.1080/014311698215027.

Negri, A. J., R. F. Adler, R. A. Maddox, K. W. Howard, and P. R. Keehn (1993), A regional rainfall climatology over Mexico and the southwest United States derived from passive microwave and geosynchronous infrared data, *J. Clim.*, *6*(11), 2144–2161, doi:10.1175/1520-0442(1993)006AP),2144:ARRCOM>2.0.CO;2.

Peel, M. C., B. L. Finlayson, and T. A. McMahon (2007), Updated world map of the Köppen-Geiger climate classification, *Hydrol. Earth Syst. Sci.*, *11*, 1633–1644.

Peters-Lidard, C. D., F. Pan, and E. F. Wood (2001), A re-examination of modeled and measured soil moisture spatial variability and its implications for land surface modeling, *Adv. Water Resour.*, *24*, 1069–1083, doi:10.1016/S0309-1708(01)00035-5.

Rawls, W. J., D. L. Brakensiek, and N. Miller (1983), Green-Ampt infiltration parameters from soil data, *J. Hydraul. Eng.*, *109*(1), 62–70, doi:10.1061/(ASCE)0733-9429(1983)109:1(62).

Rodríguez-Iturbe, I., and A. Porporato (2004), *Ecohydrology of Water-Controlled Ecosystems*, 442 pp., Cambridge Univ. Press, Cambridge, U. K.

Rodríguez-Iturbe, I., G. K. Vogel, R. Rigon, D. Entekhabi, F. Castelli, and A. Rinaldo (1995), On the spatial organization of soil moisture fields, *Geophys. Res. Lett.*, *22*(20), 2757–2760, doi:10.1029/95GL02779.

Rutter, A. J., K. A. Kershaw, P. C. Robins, and A. J. Morton (1971), A predictive model of rainfall interception in forests. 1. Derivation of the model from observation in a plantation of Corsican pine, *Agric. Meteorol.*, *9*, 367–384, doi:10.1016/0002-1571(71)90034-3.

Salinas-Zavala, C. A., A. V. Douglas, and H. F. Díaz (2002), Interannual variability of NDVI in northwest Mexico. Associated climatic mechanisms and ecological implications, *Remote Sens. Environ.*, *82*(2–3), 417–430, doi:10.1016/S0034-4257(02)00057-3.

Scott, R. L., E. A. Edwards, W. J. Shuttleworth, T. E. Huxman, C. J. Watts, and D. C. Goodrich (2004), Interannual and seasonal variations of fluxes of water and carbon dioxide from a riparian woodland ecosystem, *Agric. For. Meteorol.*, *122*, 65–84, doi:10.1016/j.agrformet.2003.09.001.

Secretaría de Infraestructura Urbana y Ecología–Instituto del Medio Ambiente y Desarrollo Sustentable del Estado de Sonora (1998), *Proyecto de Ordenamiento Ecológico del Territorio del Estado de Sonora*, 577 pp., Hermosillo, Mexico.

Secretaría de Programación y Presupuesto (1984), Carta geológica, *H12-5*, scale 1:250000, Dir. Gen. de Geogr., Mexico City.

Settin, T., G. Botter, I. Rodriguez-Iturbe, and A. Rinaldo (2007), Numerical studies on soil moisture distributions in heterogeneous catchments, *Water Resour. Res.*, *43*, W05425, doi:10.1029/2006WR005737.

Seyfried, M. S., and M. Murdock (2004), Measurement of soil water content with a 50 MHz soil dielectric sensor, *Soil Sci. Soc. Am. J.*, *68*(2), 394–403.

Sheppard, P. R., A. C. Comrie, G. D. Packin, K. Angersbach, and M. K. Hughes (2002), The climate of the US Southwest, *Clim. Res.*, *21*, 219–238, doi:10.3354/cr021219.

Shuttleworth, W. J. (1979), Evaporation, *Rep. 56*, Inst. of Hydrol, Wallingford, U. K.

Sivapalan, M. (2005), Pattern, process and function: Elements of a new unified hydrologic theory at the catchment scale, in *Encyclopedia of Hydrologic Sciences*, vol. 1, edited by M. G. Anderson, pp. 193–219, John Wiley, New York.

Small, E. E., and S. A. Kurc (2003), Tight coupling between soil moisture and the surface radiation budget in semiarid environments: Implications for land-atmosphere interactions, *Water Resour. Res.*, *39*(10), 1278, doi:10.1029/2002WR001297.

Teuling, A. J., and P. A. Troch (2005), Improved understanding of soil moisture variability dynamics, *Geophys. Res. Lett.*, *32*, L05404, doi:10.1029/2004GL021935.

Teuling, A. J., F. Hupet, R. Uijlenhoet, and P. A. Troch (2007), Climate variability effects on spatial soil moisture dynamics, *Geophys. Res. Lett.*, *34*, L06406, doi:10.1029/2006GL029080.

Vivoni, E. R., V. Y. Ivanov, R. L. Bras, and D. Entekhabi (2004), Generation of triangulated irregular networks based on hydrological similarity, *J. Hydrol. Eng.*, *9*(4), 288–302, doi:10.1061/(ASCE)1084-0699(2004)9:4(288).

Vivoni, E. R., V. Y. Ivanov, R. L. Bras, and D. Entekhabi (2005), On the effects of triangulated terrain resolution on distributed hydrologic model response, *Hydrol. Processes*, *19*, 2101–2122, doi:10.1002/hyp.5671.

Vivoni, E. R., D. Entekhabi, R. L. Bras, V. Y. Ivanov, M. P. Van Horne, C. Grassotti, and R. N. Hoffman (2006), Extending the predictability of hydrometeorological flood events using radar rainfall nowcasting, *J. Hydrometeorol.*, *7*(4), 660–677, doi:10.1175/JHM514.1.

Vivoni, E. R., D. Entekhabi, R. L. Bras, and V. Y. Ivanov (2007a), Controls on runoff generation and scale-dependence in a distributed hydrologic model, *Hydrol. Earth Syst. Sci.*, *11*(5), 1683–1701.

Vivoni, E. R., et al. (2007b), Variation of hydrometeorological conditions along a topographic transect in northwestern Mexico during the North American monsoon, *J. Clim.*, *20*(9), 1792–1809, doi:10.1175/JCLI4094.1.

Vivoni, E. R., M. Gebremichael, C. J. Watts, R. Bindlish, and T. J. Jackson (2008a), Comparison of ground-based and remotely sensed surface soil moisture estimates over complex terrain during SMEX04, *Remote Sens. Environ.*, *112*(2), 314–325, doi:10.1016/j.rse.2006.10.028.

Vivoni, E. R., H. A. Moreno, G. Mascaro, J. C. Rodríguez, C. J. Watts, J. Garatuza-Payan, and R. Scott (2008b), Observed relation between evapotranspiration and soil moisture in the North American monsoon region, *Geophys. Res. Lett.*, *35*, L22403, doi:10.1029/2008GL036001.

Vivoni, E. R., et al. (2008c), Vegetation controls on soil moisture distribution in the Valles Caldera, New Mexico, during the North American monsoon, *Ecohydrology*, *1*(3), 225–238, doi:10.1002/eco.11.

Vivoni, E. R., F. Di Benedetto, S. Grimaldi, and E. A. B. Eltahir (2008d), Hypsometric control on surface and subsurface runoff, *Water Resour. Res.*, *44*, W12502, doi:10.1029/2008WR006931.

Vivoni, E. R., C. J. Watts, J. C. Rodríguez, J. Garatuza-Payan, L. A. Méndez-Barroso, and J. A. Saiz-Hernández (2010), Improved land-atmosphere relations through distributed footprint measurements in a subtropical scrubland during the North American monsoon, *J. Arid Environ.*, doi:10.1016/j.jaridenv.2009.09.031, in press.

Watts, C. J., R. L. Scott, J. Garatuza-Payan, J. C. Rodríguez, J. H. Prueger, W. P. Kustas, and M. Douglas (2007), Changes in vegetation condition and surface fluxes during NAME 2004, *J. Clim.*, *20*(9), 1810–1820, doi:10.1175/JCLI4088.1.

Western, A. W., and R. B. Grayson (2000), Soil moisture and runoff processes at Tarrawara, in *Spatial Patterns in Catchment Hydrology—Observations and Modelling*, edited by R. B. Grayson and G. Bloschl, pp. 209–246, Cambridge Univ. Press, Cambridge, U. K.

Western, A. W., R. B. Grayson, G. Bloschl, G. R. Willgoose, and T. A. McMahon (1999), Observed spatial organization of soil moisture and its relation to terrain indices, *Water Resour. Res.*, *35*(3), 797–810, doi:10.1029/1998WR900065.

Wierenga, P. J., J. M. H. Hendrickx, M. H. Nash, J. Ludwig, and L. A. Daugherty (1987), Variation of soil and vegetation with distance along a transect in the Chihuahuan desert, *J. Arid Environ.*, *13*(1), 53–63.

Wilson, D. J., A. W. Western, and R. B. Grayson (2004), Identifying and quantifying sources of variability in temporal and spatial soil moisture observations, *Water Resour. Res.*, *40*, W02507, doi:10.1029/2003WR002306.

Wooldridge, S. A., J. D. Kalma, and J. P. Walker (2003), Importance of soil moisture measurements for inferring parameters in hydrologic models of low-yielding ephemeral catchments, *Environ. Model. Softw.*, *18*, 35–48, doi:10.1016/S1364-8152(02)00038-5.

Yépez, E. A., E. R. Vivoni, C. J. Watts, J. C. Rodríguez, J. Garatuza-Payan, L. A. Méndez-Barroso, J. Saiz-Hernandez, and D. J. Gochis (2008), *Componentes de la Evapotranspiración en Matorrales Xerófilos de Sonora en un Contexto Ecohidrológico*, Soc. Cient. Mex. de Ecol., Merida, Mexico.

Yilmaz, M. T., E. R. Hunt, L. D. Goins, S. L. Ustin, V. C. Venderbilt, and T. J. Jackson (2008), Vegetation water content during SMEX04 from ground data and Landsat 5 Thematic Mapper imagery, *Remote Sens. Environ.*, *112*, 350–362, doi:10.1016/j.rse.2007.03.029.

Zhu, C., and D. P. Lettenmaier (2007), Long-term climate and derived surface hydrology and energy flux data for Mexico: 1925–2004, *J. Clim.*, *20*(9), 1936–1946, doi:10.1175/JCLI4086.1.

J. C. Rodríguez, Departamento de Agricultura y Ganadería, Universidad de Sonora, Hermosillo, Sonora 83100, Mexico.

E. R. Vivoni, School of Earth and Space Exploration, Arizona State University, Bateman Physical Science Center, F-Wing, Room 650A, Tempe, AZ 85287-1404, USA. (vivoni@asu.edu)

C. J. Watts, Departamento de Física, Universidad de Sonora, Hermosillo, Sonora 83100, Mexico.